Science Advances
AAAS

Supplementary Materials for

Nitroreductase-instructed supramolecular assemblies for microbiome regulation to enhance colorectal cancer treatments

Jiali Chen *et al.*

Corresponding author: Yuan Gao, gaoy@nanoctr.cn

Sci. Adv. **8**, eadd2789 (2022)
DOI: 10.1126/sciadv.add2789

This PDF file includes:

1. Chemical Synthesis

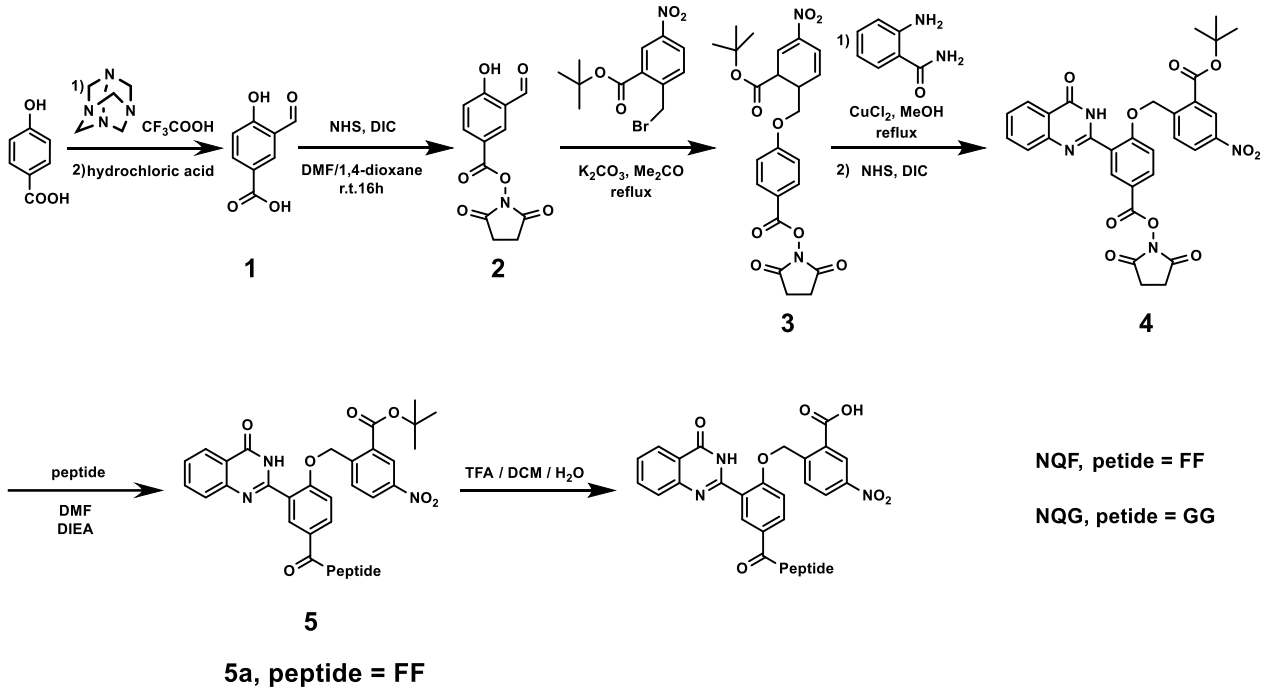

1.1 Synthesis of 3-formyl-4-hydroxybenzoic acid (compound 1)

According to previous report *(36)*, 4-Hydroxybenzoic acid (15 g; 108 mmol) was suspended in 40 mL of trifluoroacetic acid. Hexamethylenetetramine (15.3 g; 109 mmol) was dissolved in 45 mL of trifluoroacetic acid. Then the solution of hexamethylenetetramine was added dropwise into the suspension of 4-hydroxybenzoic. The mixture was refluxed for 2 hours. After cooling to room temperature, the mixture was added into 300 mL of 4 M HCl and stirred for another 3 h. The yellow precipitate was then isolated by filtration and washed by water. The yellow solid was dried under vacuum yielding **1** (5.77 g, 32%) without other purification. ^{1}H NMR (400 MHz, DMSO-d6) δ (ppm): 12.83 (s, 1H), 11.47 (s, 1H), 10.36 -10.20 (m, 1H), 8.24 (d, *J* = 2.2 Hz, 1H), 8.04 (dd, *J* = 8.7, 2.4 Hz, 1H), 7.09 (d, *J* = 8.6 Hz, 1H).

1.2 Synthesis of N-Sucdnimidyt 3-Formyl-4-hydroxyhenzoate (compound 2)

According to previous report *(37)*, Compound 1 (800 mg, 4.8 mmol) was firstly dissolved in the minimal amount of DMF. Then the solution of compound 1 was added with the solution of N-hydroxysuccinimide (828.2 mg, 7.2 mmol) in 1,4-dioxane at room temperature. A solution of DIC (1.115 mL) in dioxane was added into the mixture for 18h at room temperature. The white solid was removed by filtration, the solvent was removed by evaporation and purified by column chromatography (petroleum ether/EtOAc = 3/1) to provide **compound 2** (972.19 mg, 77%). ^{1}H NMR (400 MHz, DMSO-d6) δ (ppm): 12.04 (s, 0H), 10.29 (s, 1H), 8.31 (d, J = 2.3 Hz, 1H), 8.14 (dd, J = 8.9, 2.2 Hz, 1H), 7.19 (d, J = 8.8 Hz, 1H), 2.85 (s, 4H).

1.3 Synthesis of tert-butyl 2-((4-(((2,5-dioxopyrrolidin-1-yl)oxy)carbonyl)-2-formylphenoxy)methyl)-5-nitrobenzoate (compound 3)

Compound **2** (789.12 mg, 3.0 mmol) was suspended in acetone (15 mL) with tert-butyl 2-(bromomethyl)-5-nitrobenzoate (945.03 mg, 3.0 mmol) and K_2CO_3 (414.6 mg, 3.0 mmol), the

mixture was refluxed for 4 h. After cooling to room temperature, the solvent was removed by evaporation. The crude product was purified by column chromatography (petroleum ether/EtOAc = 3/1) to provide yellow solid as **compound 3** (933.69 mg, 62.48 %). ^{1}H NMR (400 MHz, DMSO-d6) δ (ppm): 10.43 (s, 1H), 8.62 (d, *J* = 2.6 Hz, 1H), 8.51 - 8.46 (m, 1H), 8.41 (d, *J* = 10.1 Hz, 2H), 8.15 (d, *J* = 8.6 Hz, 1H), 7.55 (d, *J* = 8.8 Hz, 1H), 5.84 (s, 2H), 2.90 (s, 4H), 1.55 (s, 9H).

1.4 Synthesis of 4-((2-(tert-butoxycarbonyl)-4-nitrobenzyl)oxy)-3-(4-oxo-3,4-dihydroquinazolin-2-yl)benzoic acid (compound 4)

Compound **3** (273.97 mg, 0.55 mmol), 2-aminobenzamide (68.04 mg, 0.5 mmol) and $CuCl_2$ (67.23 mg, 0.5 mmol) were suspended in 10 mL MeOH. The mixture was refluxed for 6 h and then cooled to room temperature. White powder precipitate formed while cooling down. The precipitate was collected by filtration and washed with MeOH for three times. The dried powder was then dissolved in 10 mL DMF. NHS (172.64 mg, 1.5 mmol) and DIC (23 μL) was added into the solution and stirred at 30 °C overnight. The mixture was extracted with EtOAc and purified by column chromatography (petroleum ether/EtOAc = 1/1) to give yellow powder (238.83mg, 77.78%). ^{1}H NMR (400 MHz, DMSO-d6) δ (ppm): 12.48 (s, 1H), 8.59 (d, *J* = 2.5 Hz, 1H), 8.42 (d, *J* = 2.4 Hz, 1H), 8.35 (dd, *J* = 8.6, 2.6 Hz, 1H), 8.31 (dd, *J* = 8.9, 2.4 Hz, 1H), 8.19 (dd, *J* = 7.9, 1.6 Hz, 1H), 7.99 (d, *J* = 8.7 Hz, 1H), 7.88 (ddd, *J* = 8.4, 7.0, 1.6 Hz, 1H), 7.83 - 7.76 (m, 1H), 7.62 - 7.56 (m, 1H), 7.48 (d, *J* = 8.9 Hz, 1H), 5.79 (s, 2H), 2.91 (s, 4H), 1.56 (s, 9H).

1.5 Synthesis of NQF and NQG

1.5.1 Synthesis of NQF

Compound **4** (64.4mg, 0.1mmol) was dissolved in 10 mL DMF. 3 e.q. dipeptide FF was dissolved in minimum amount of H_2O with 3 e.q. DIEA. Then solution of compound **4** was added with peptide solution and stirred at 50 °C overnight. The mixture was extracted with DCM. The solvent of the combined organic phase was removed by evaporation and purified by column chromatography (DCM/MeOH = 15/1) to give **compound 5a**.

Then the obtained **5a** was dissolved in 5 mL cleavage solution (TFA/DCM/H_2O = 90/5/5) and stirred at room temperature overnight. The solution was dropped into ice diethyl ether dropwise to give a white precipitate. **NQF** was collected by centrifuge and dried for further test.

5a (44.38mg, 54.7%**):** 8.62 (d, *J* = 8.7 Hz, 1H), 8.57 (d, *J* = 2.5 Hz, 1H), 8.36 - 8.31 (m, 2H), 8.21 - 8.15 (m, 2H), 8.01 - 7.94 (m, 2H), 7.88 (t, *J* = 7.9 Hz, 1H), 7.78 (d, *J* = 8.1 Hz, 1H), 7.57 (t, *J* = 7.5 Hz, 1H), 7.33 (d, *J* = 7.6 Hz, 2H), 7.29 - 7.09 (m, 10H), 5.68 (s, 2H), 4.76 (d, *J* = 7.8 Hz, 1H), 4.52 - 4.44 (m, 1H), 3.09 (dd, *J* = 13.8, 5.2 Hz, 2H), 3.01 - 2.92 (m, 2H), 1.54 (s, 9H).

NQF (36.97mg, 89.5%**):** 8.67 (d, *J* = 2.5 Hz, 1H), 8.61 (d, *J* = 8.6 Hz, 1H), 8.36 - 8.29 (m, 2H), 8.19 (dd, *J* = 8.4, 1.8 Hz, 2H), 7.95 (dd, *J* = 8.7, 2.4 Hz, 2H), 7.88 (ddd, *J* = 8.5, 7.1, 1.6 Hz, 1H), 7.79 (d, *J* = 8.1 Hz, 1H), 7.61- 7.53 (m, 1H), 7.35 - 7.30 (m, 2H), 7.27 - 7.11 (m, 10H), 5.76 (s, 2H), 4.82 - 4.71 (m, 1H), 4.48 (td, *J* = 8.2, 5.1 Hz, 1H), 3.09 (dd, *J* = 13.9, 5.0 Hz, 2H), 2.96 (ddd, *J* = 14.0, 5.8, 3.1 Hz, 2H).

1.5.2 Synthesis of NQG

Compound **4** (64.4mg, 0.1mmol) was dissolved in 10 mL DMF. 3 e.q. dipeptides GG was dissolved in minimum amount of H_2O with 3 e.q. DIEA. Then solution of compound 4 was added with peptides solution and stirred at 50 °C overnight. The mixture was subjected to semi

preparative HPLC. The dried powder was dissolved in 5 mL cleavage solution (TFA/DCM/H_2O = 90/5/5) and stirred at room temperature overnight and dropped into ice diethyl ether dropwise to give a white precipitate. **NQG** was collected by centrifuge and dried for further test.
NQG(28.96mg, 50.35%): 12.42 (s, 1H), 8.84 (t, *J* = 5.9 Hz, 1H), 8.67 (d, *J* = 2.5 Hz, 1H), 8.33 (dd, *J* = 8.7, 2.5 Hz, 1H), 8.30 (d, *J* = 2.3 Hz, 1H), 8.24 (t, *J* = 5.8 Hz, 1H), 8.18 (d, *J* = 1.5 Hz, 1H), 8.08 (dd, *J* = 8.7, 2.4 Hz, 1H), 7.97 (d, *J* = 8.7 Hz, 1H), 7.88 (td, *J* = 7.7, 7.1, 1.6 Hz, 1H), 7.79 (d, *J* = 8.1 Hz, 1H), 7.60 – 7.53 (m, 1H), 7.27 (d, *J* = 8.9 Hz, 1H), 5.77 (s, 2H), 3.92 (d, *J* = 5.8 Hz, 2H), 3.78 (d, *J* = 5.8 Hz, 2H).

2. Supporting Figures

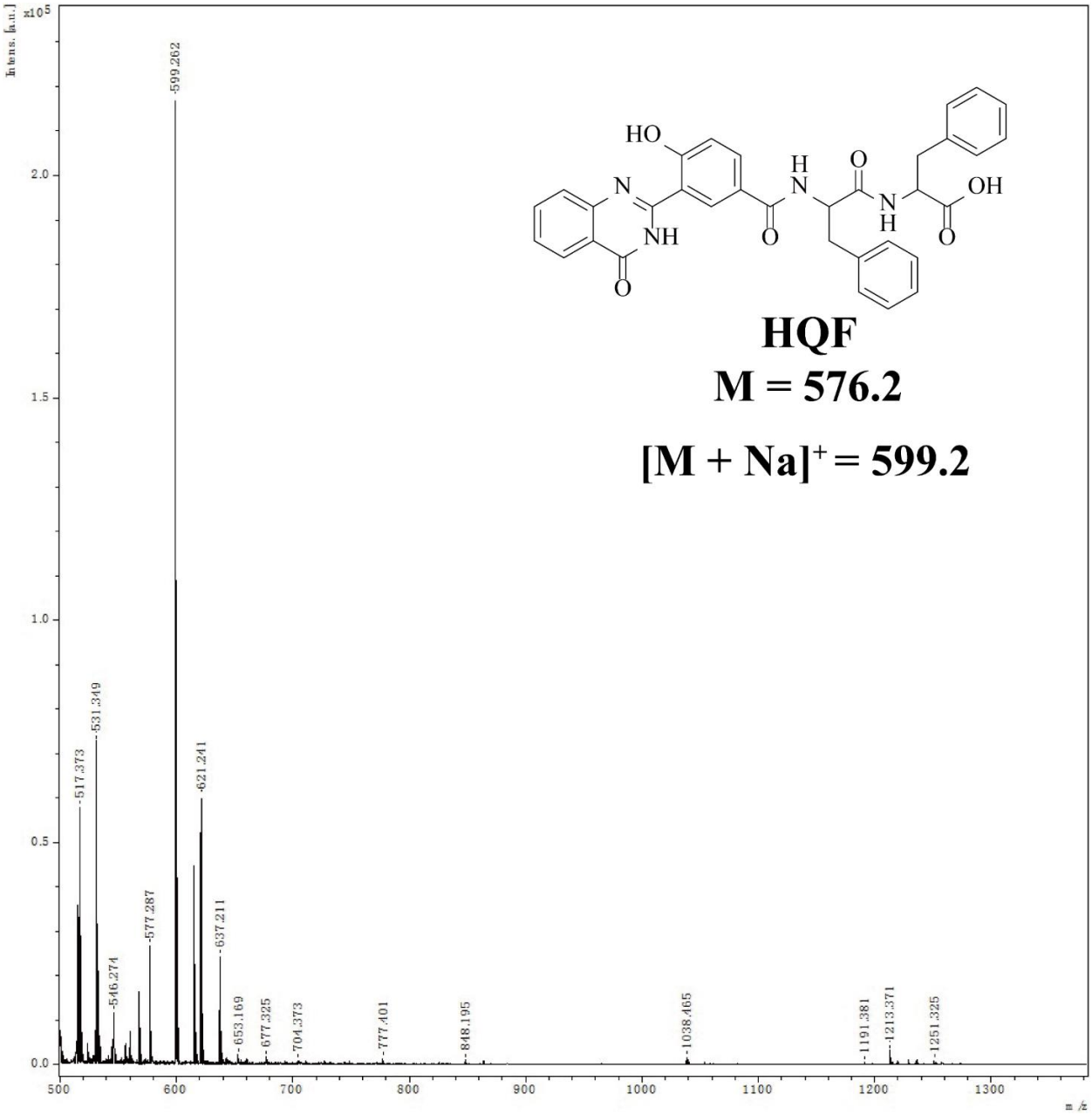

Fig. S1. MALDI-TOF mass spectrum of the peak with retention time = 15.44 min in Figure 3B.

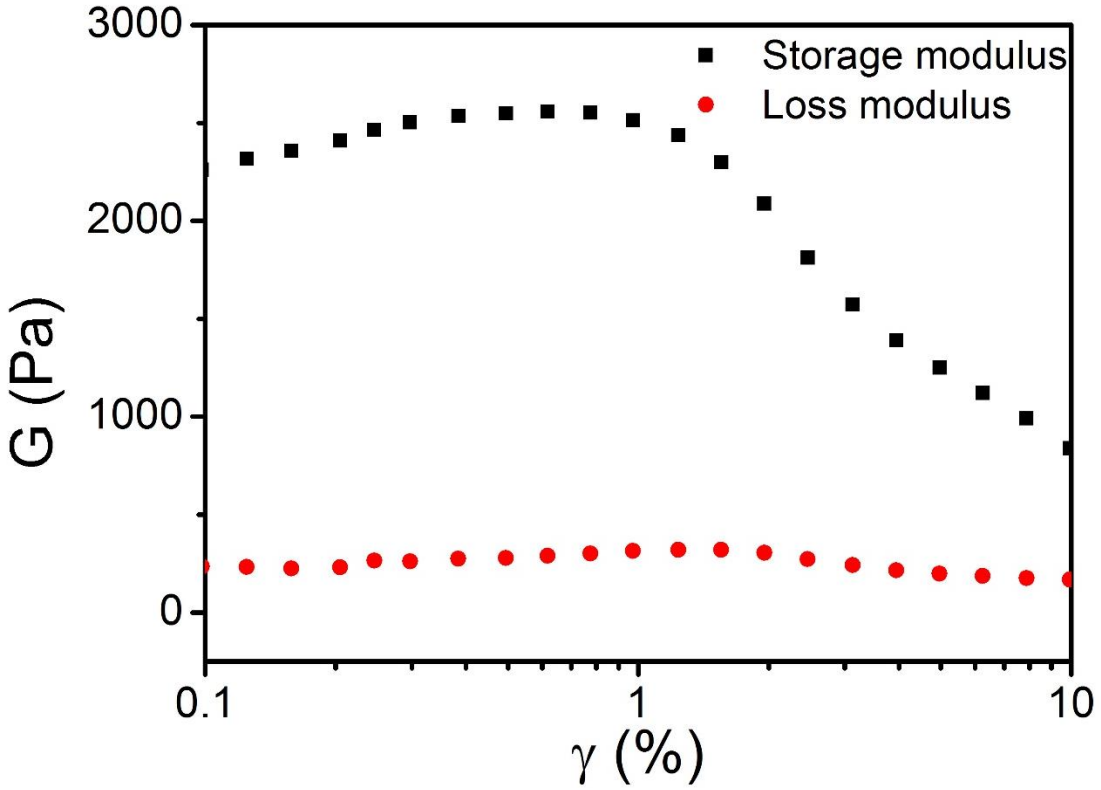

Fig. S2. Strain sweeps of the dynamic storage modulus (G') and the loss modulus (G'') of the **HQF** hydrogel.

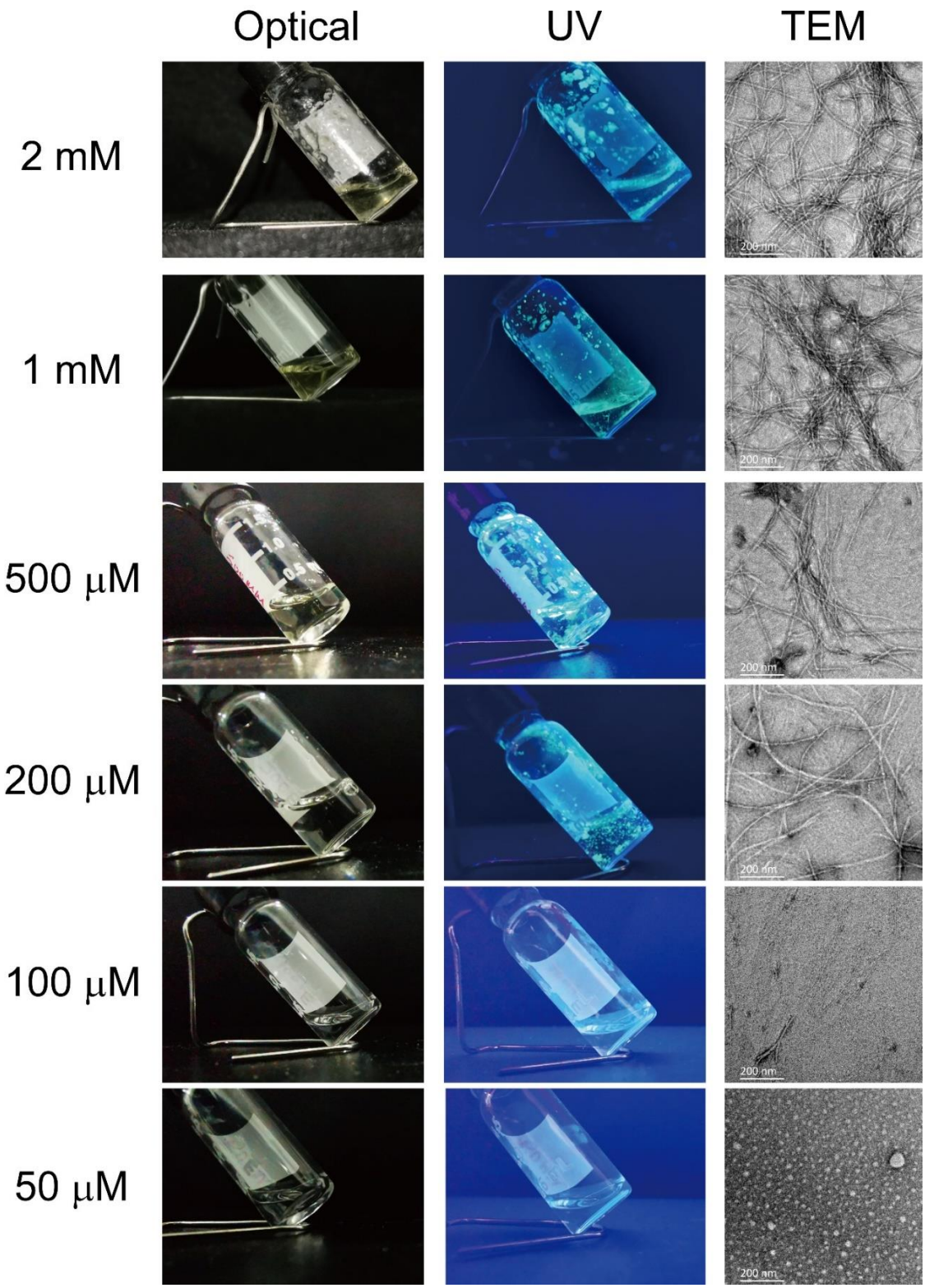

Fig. S3. Optical images w/o UV light and TEM images of **NQF** at different concentrations and incubated with NTR and NADH. (Scale bars: 200 nm)

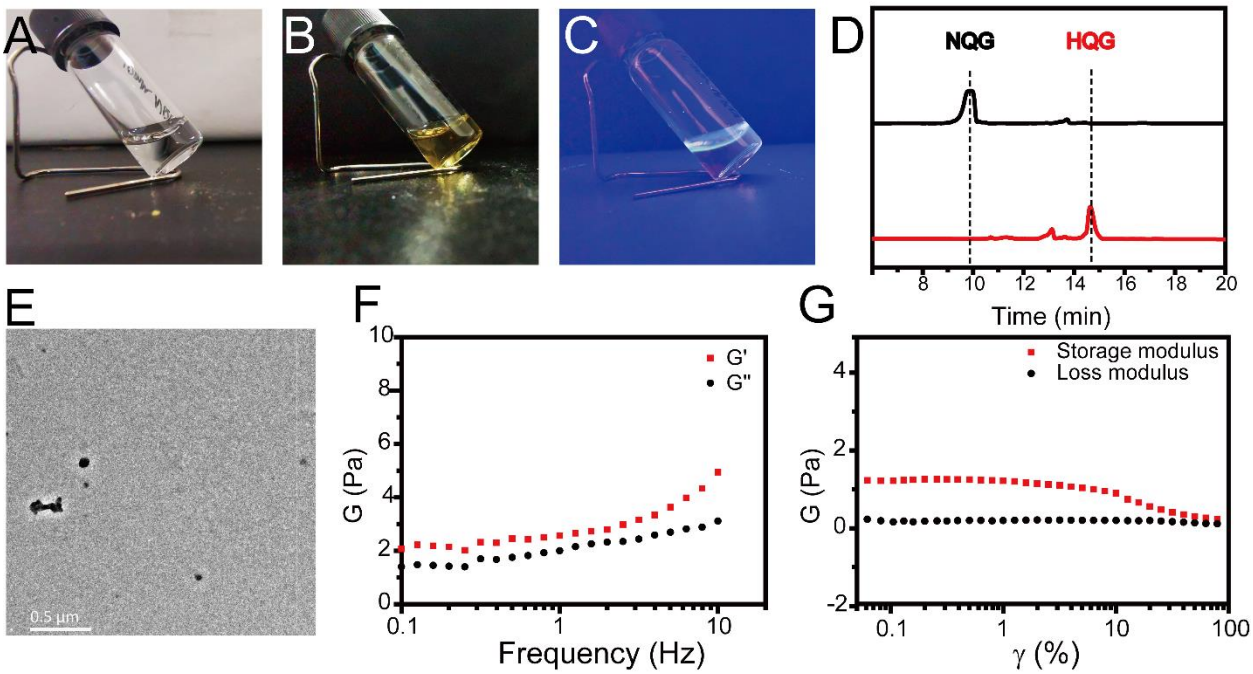

Fig. S4. Characterization of **NQG** (10 mM) incubated with NTR (10 μg) and NADH (10 e.q.). Optical images of (**A**) **NQG** and (**B**) **HQG**. (**C**) Image of **HQG** under UV light. (**D**) HPLC trace of the reduction from **NQG** to **HQG** *in vitro* with the presence of NTR / NADH. (**E**) TEM images of **HQG** solution. (**F**) Frequency sweeps and (**G**) Strain sweeps of the dynamic storage modulus (G') and loss modulus (G'') of **HQG** solution.

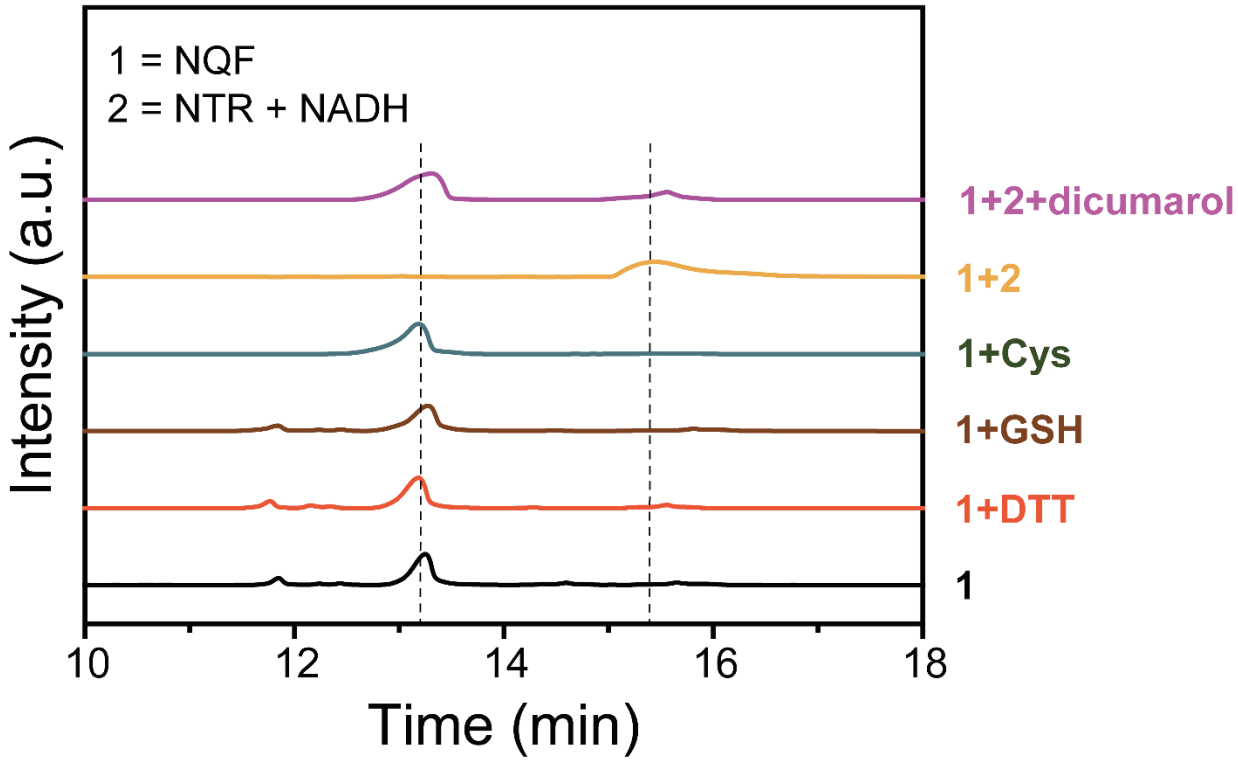

Fig. S5. HPLC trace of 1 mM **NQF** with different treatment (1 mM DTT, 1 mM GSH, 1 mM Cys, 2 μg/ml NTR+ 10 e.q. NADH, 2 μg/ml NTR +10 e.q. NADH + 500 μM dicumarol)

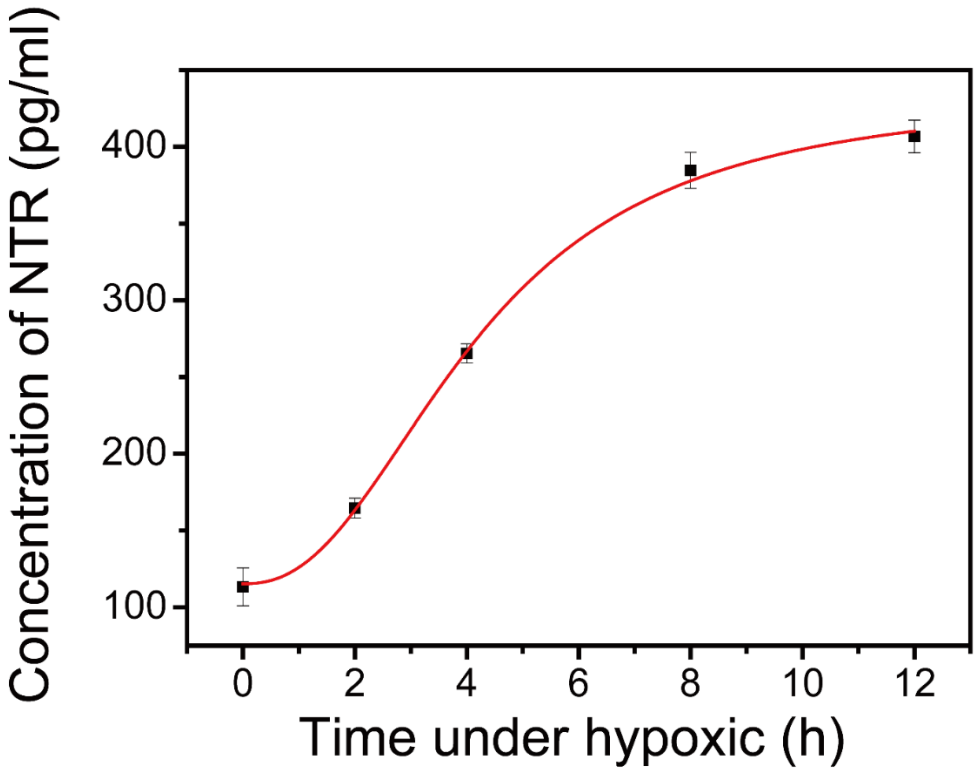

Fig. S6. The time-dependent accumulation of NTR produced by HeLa cells under hypoxic condition.

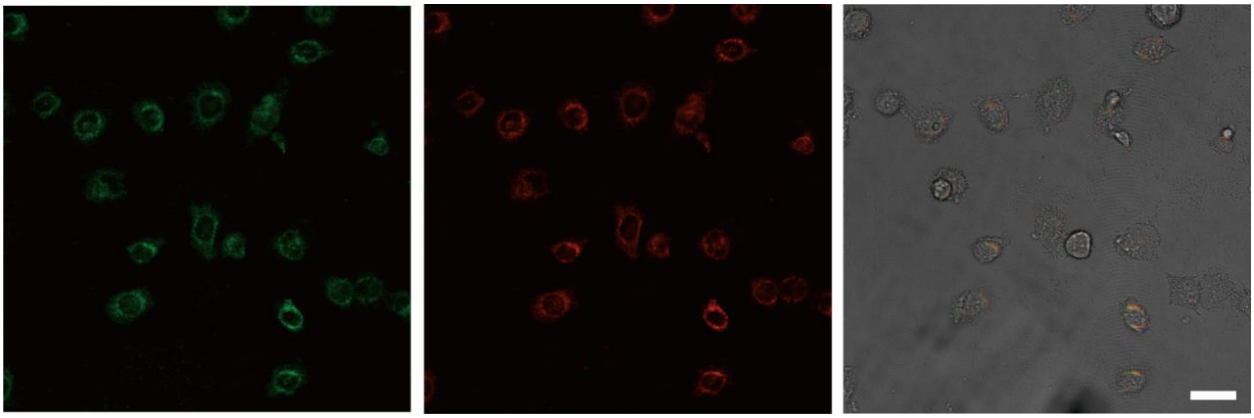

Fig. S7. Fluorescence emission from **HQF** located at mitochondria by CLSM images. Green channel indicated the emission of **HQF**. Red channel indicated the MitoTracker staining. The merged channel indicated the overlay of green / red channel and bright field. (Scale bar: 40 μm)

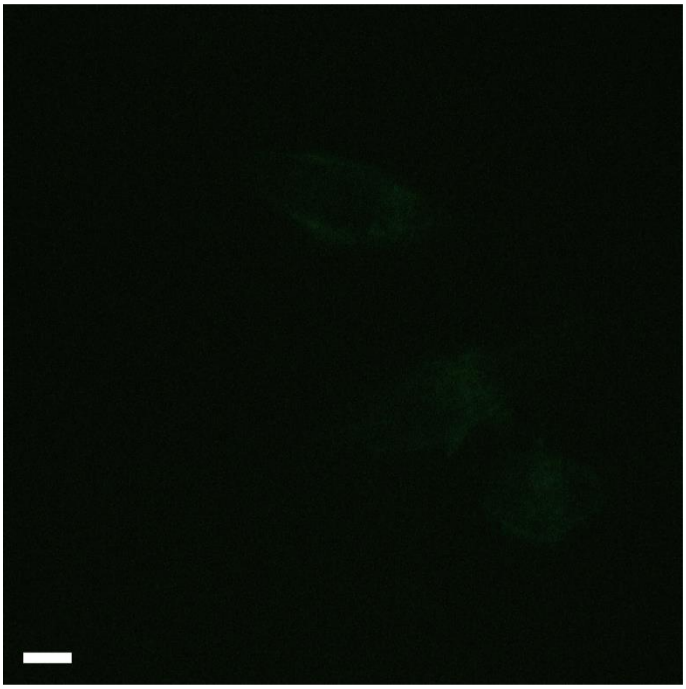

Fig. S8. Absence of fluorescence in hypoxic HeLa cells in the presence of 500 μM dicoumarol. (Scale bar: 10 μm)

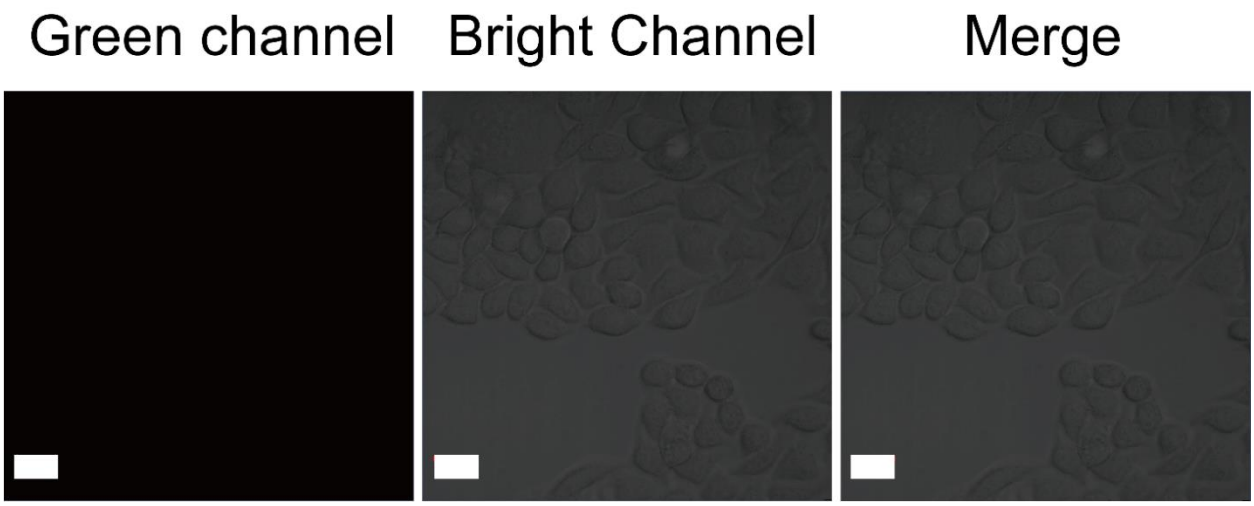

Fig. S9. CLSM images of HeLa cells treated with **NQF** under normoxic condition. (Scale bars: 20 μm)

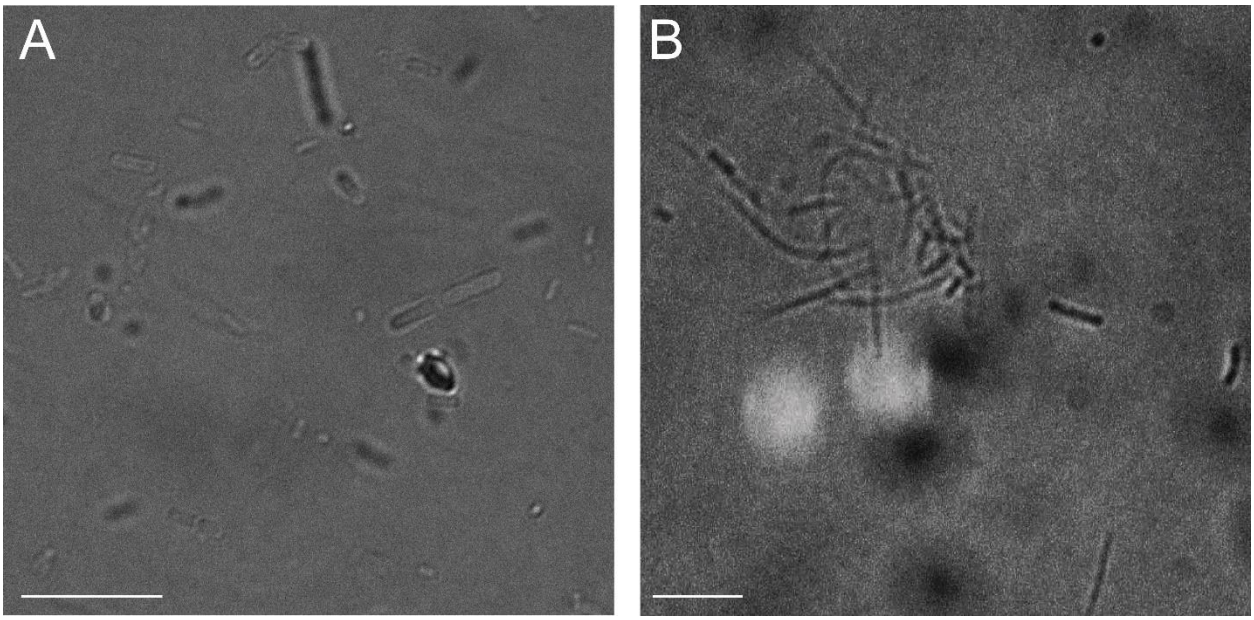

Fig S10. Corresponding DIC images of (A) *E. coli* and (B) *F. nucleatum* incubated with **NQF**. (Scale bars: 10 μm).

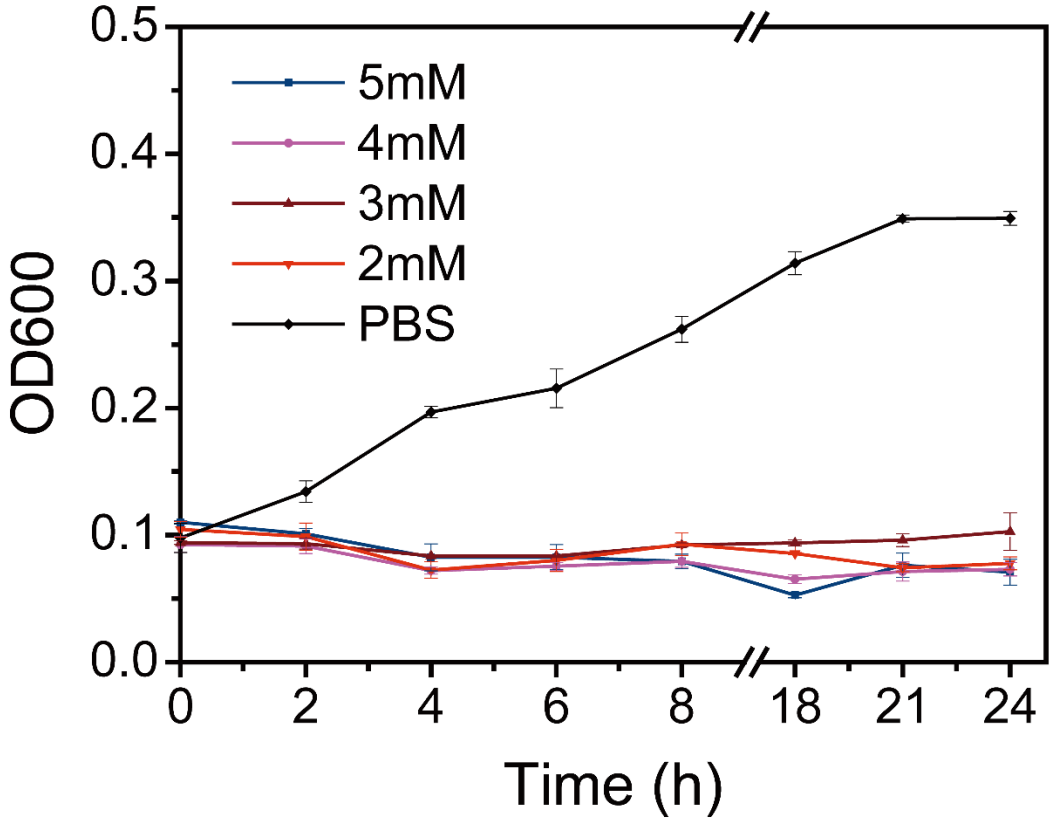

Fig. S11. Antibacterial activity of **HQF** assemblies against *F. nucleatum*.

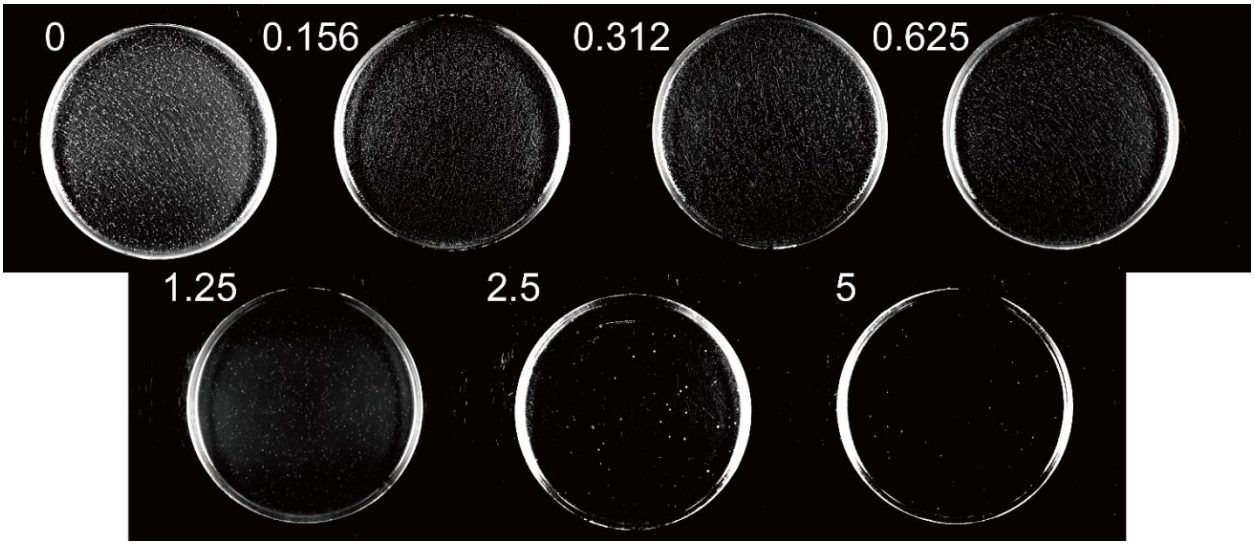

Fig. S12. Antibacterial effect of **HQF** assemblies after 24 h by spread plate of *F. nucleatum*. (Concentration unit, mM)

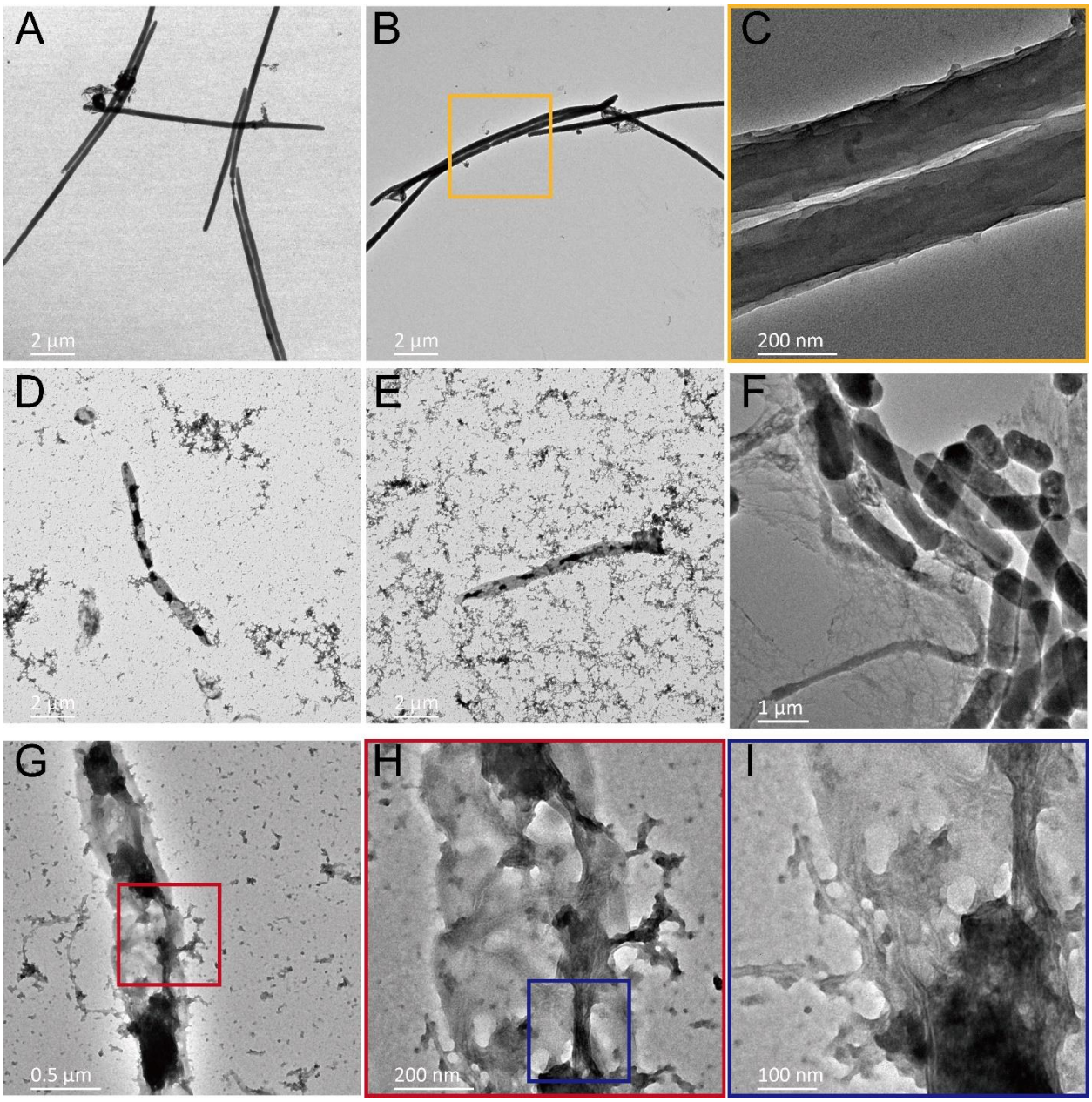

Fig. S13. TEM images of *F. nucleatum* cells. The bacteria were incubated with (**A**-**C**) PBS and (**D**-**I**) **HQF** assemblies after 24 h.

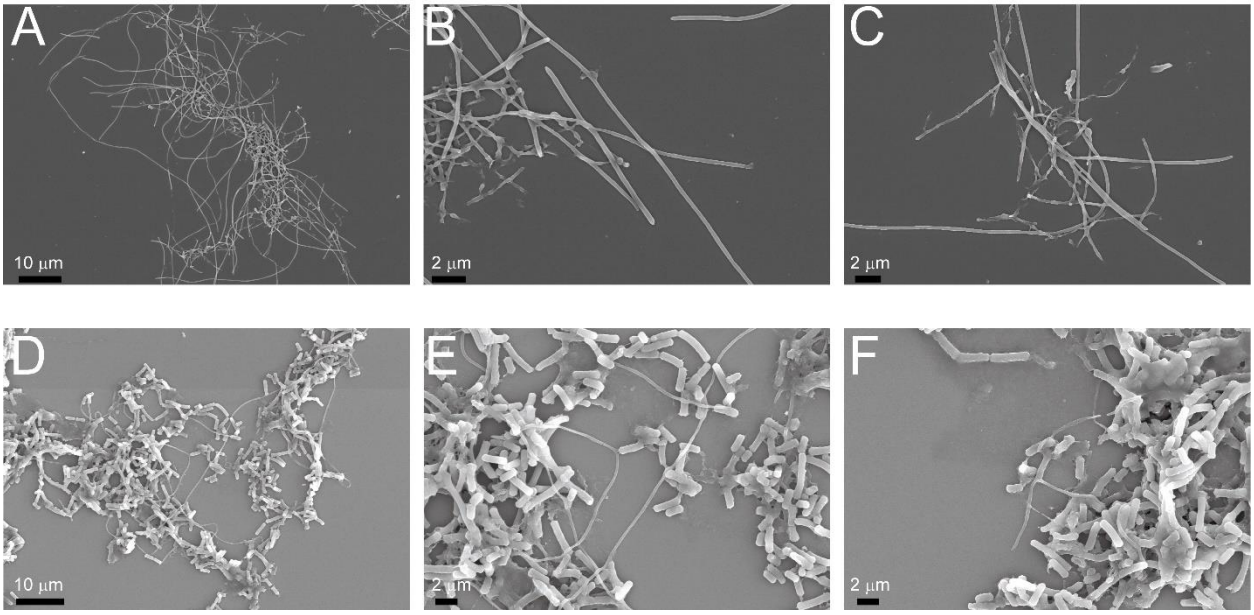

Fig. S14. SEM images of *F. nucleatum* cells treated with (**A**-**C**) PBS and (**D**-**F**) **HQF** assemblies.

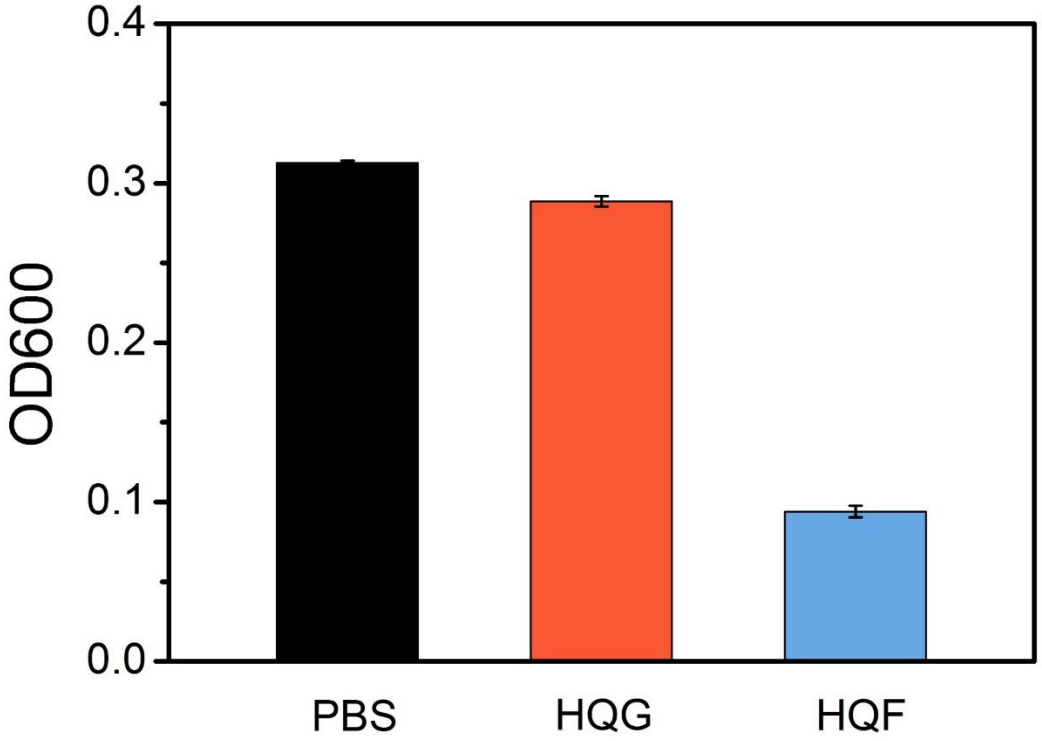

Fig. S15. Antibacterial activity of **HQG** (5 mM) and **HQF** (5 mM) against *F. nucleatum* after 24 h.

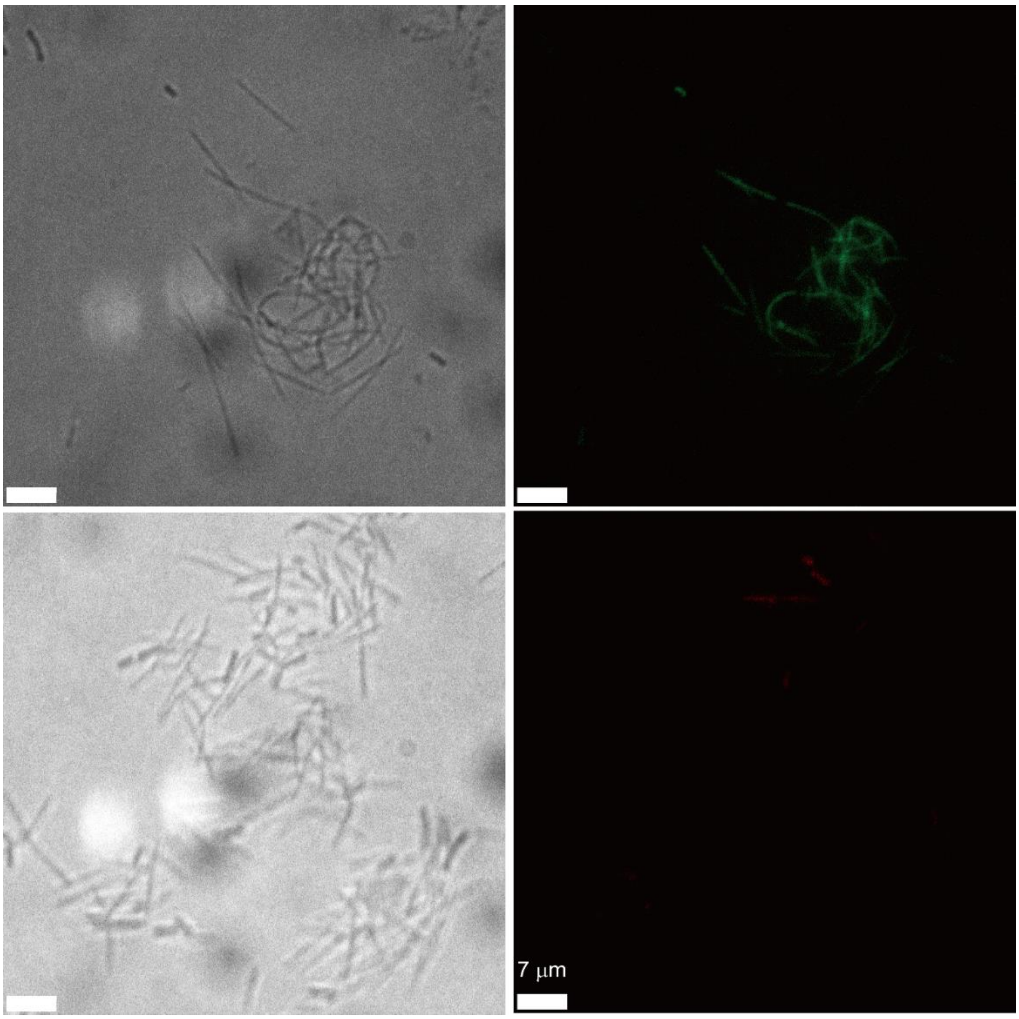

Fig. S16. Live/Dead staining of *F. nucleatum* cells treated with **HQG** solution. FM 4-64 staining (green) represented the live cells while PI (red) represented dead cells.

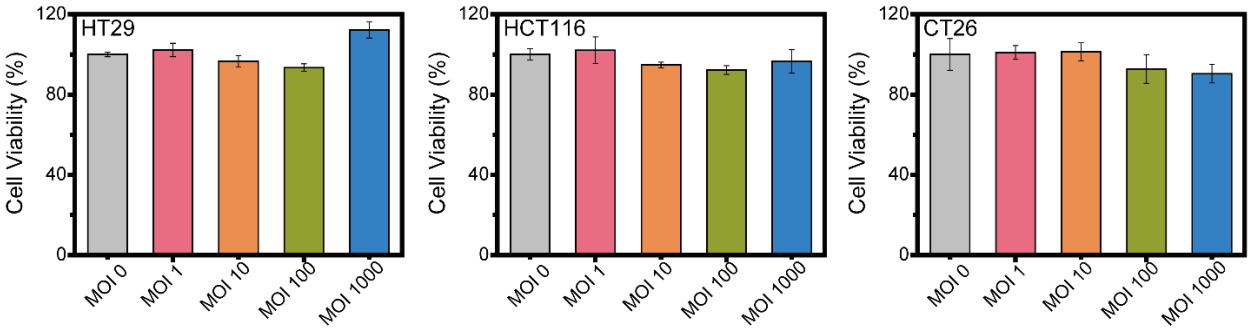

Fig. S17. Cell viability of HT29 (left), HCT116 (medium) and CT26 (right) co-cultured with *F. nucleatum* at different MOIs.

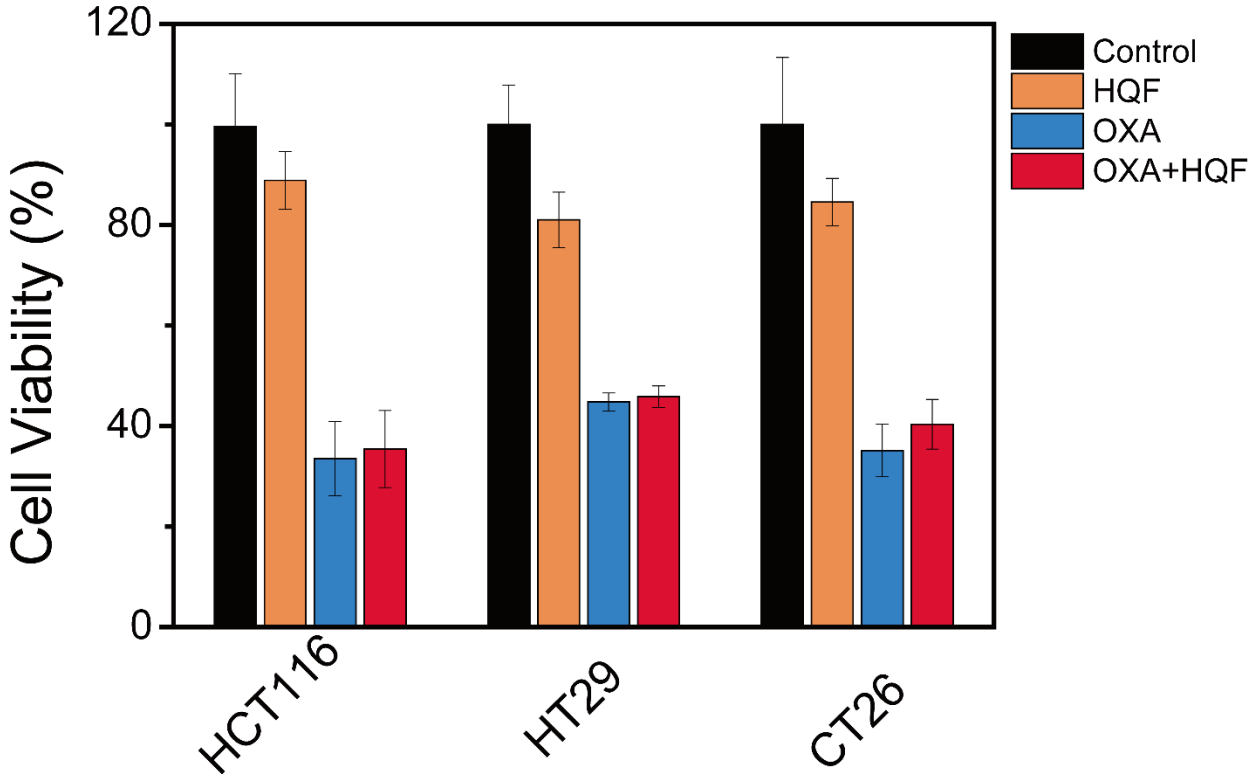

Fig S18. The effect of **HQF** on CRC cells viability under different treatments.

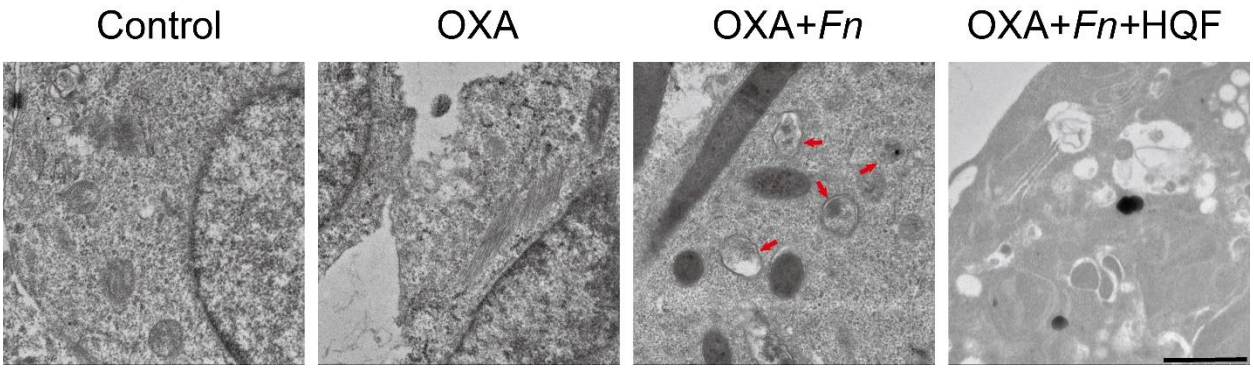

Fig S19. TEM images of autophagosomes in HCT116 cells with different treatment for 6 h. Red arrows indicated the autophagosomes. (Scale bar: 1 μm)

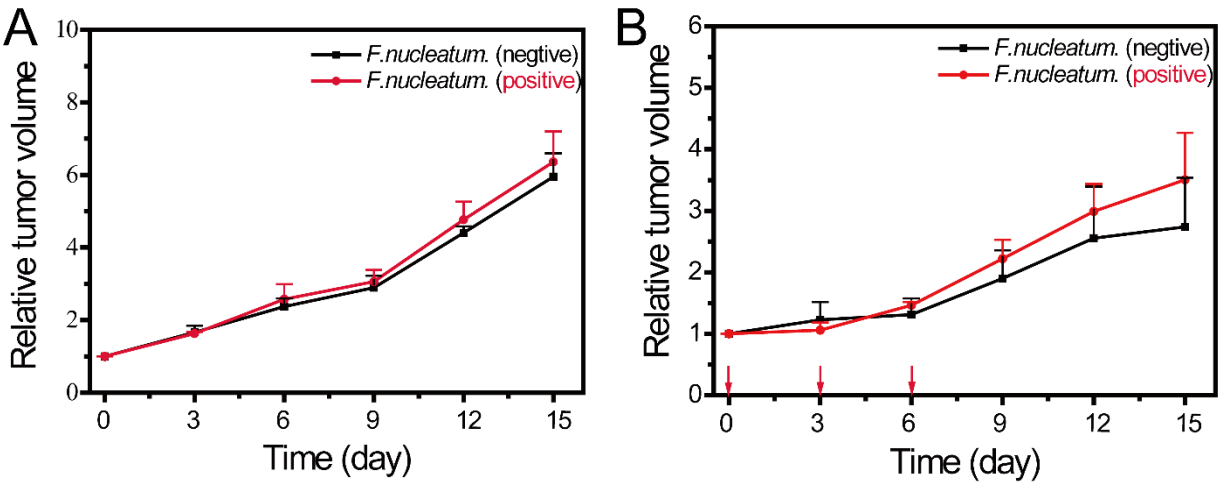

Fig. S20. The influence of *F. nucleatum* in HCT116 tumor growth (**A**) without chemo agents and (**B**) with 7.5 mg/kg OXA treatment.

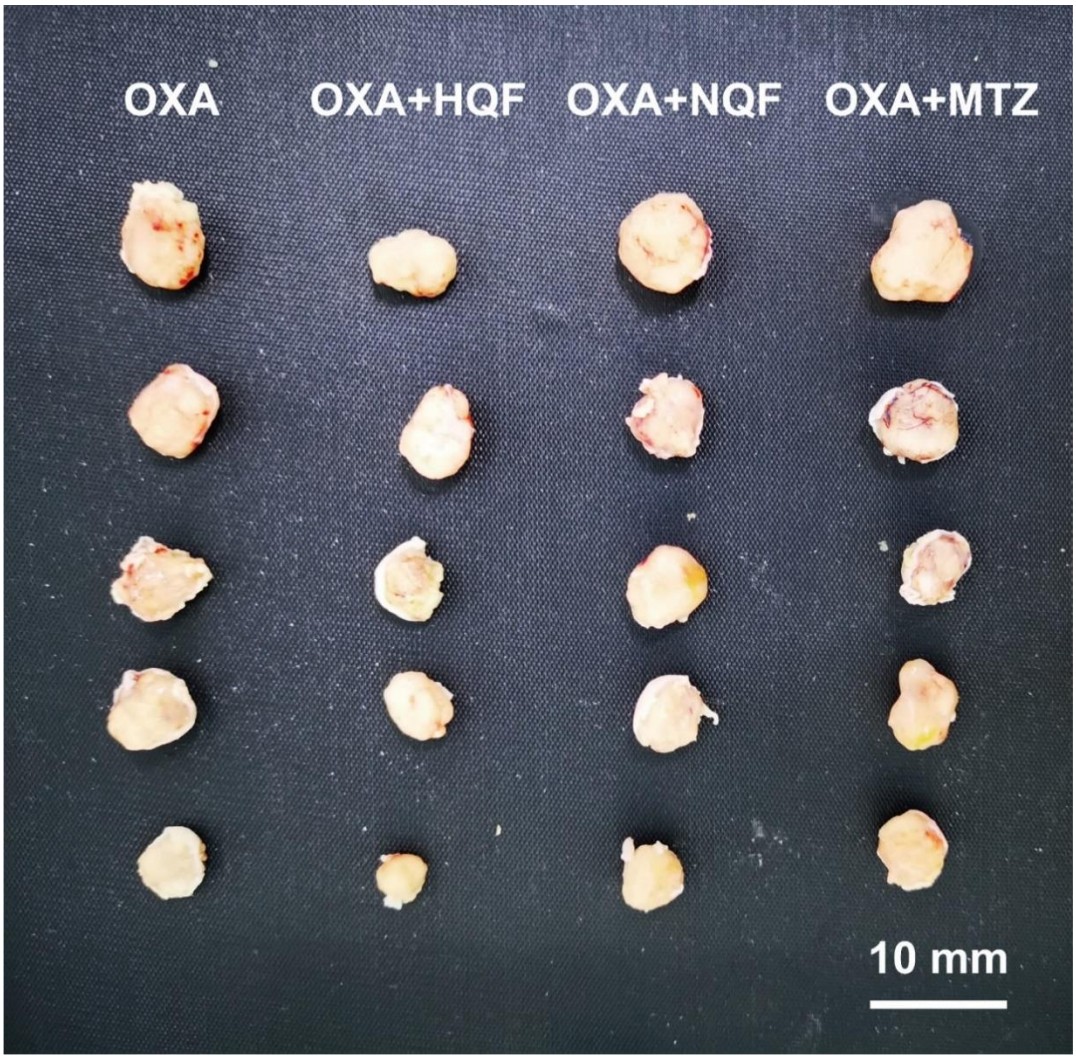

Fig. S21. Optical image of dissected tumors in each group with stated treatments. (Scale bar: 10 mm)

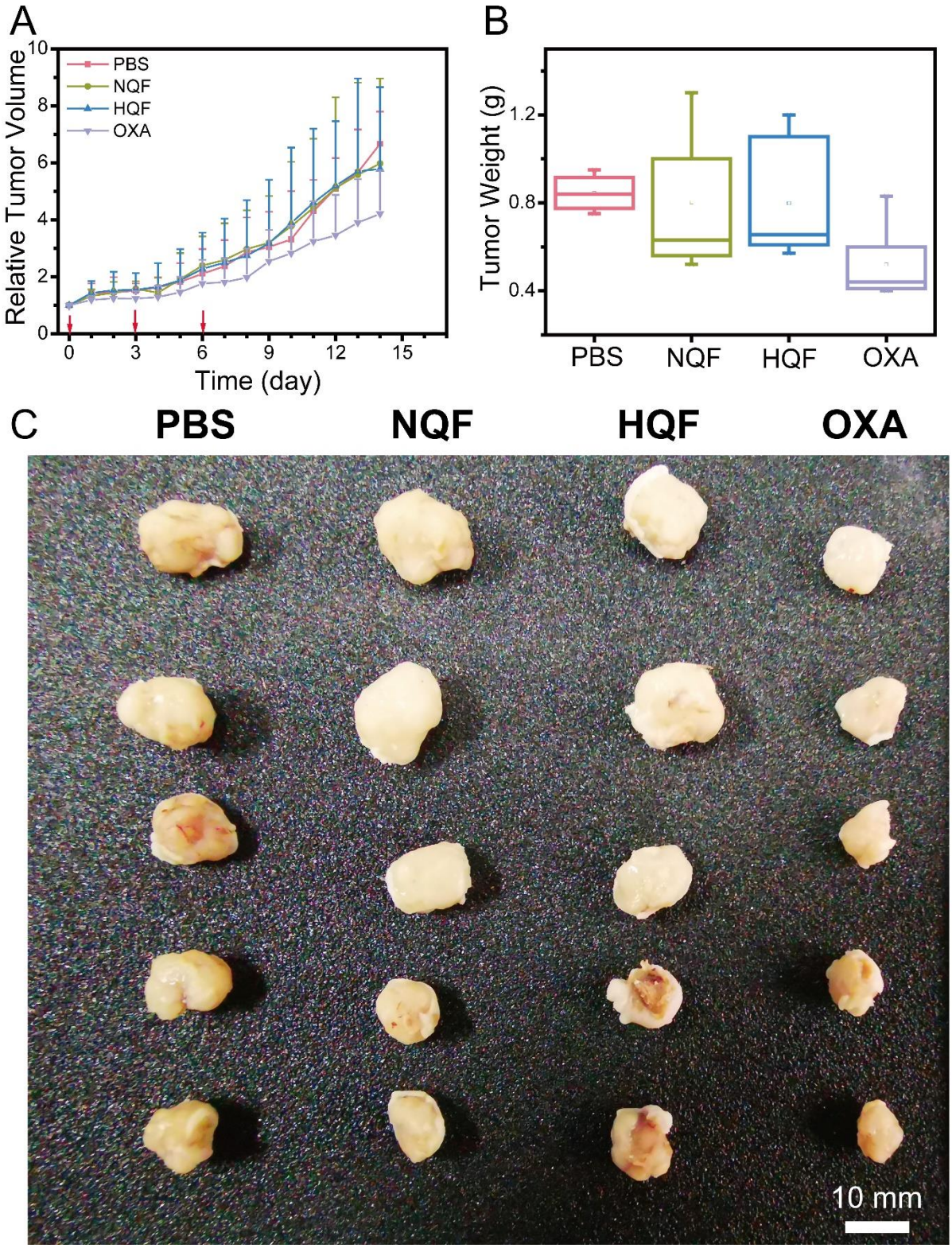

Fig. S22. Representative data of tumors in different treatment groups. (**A**) The tumor growth in each group and (**B**) tumor weight. (**C**) Representative image of dissected tumors in each group. (Scale bar: 10 mm)

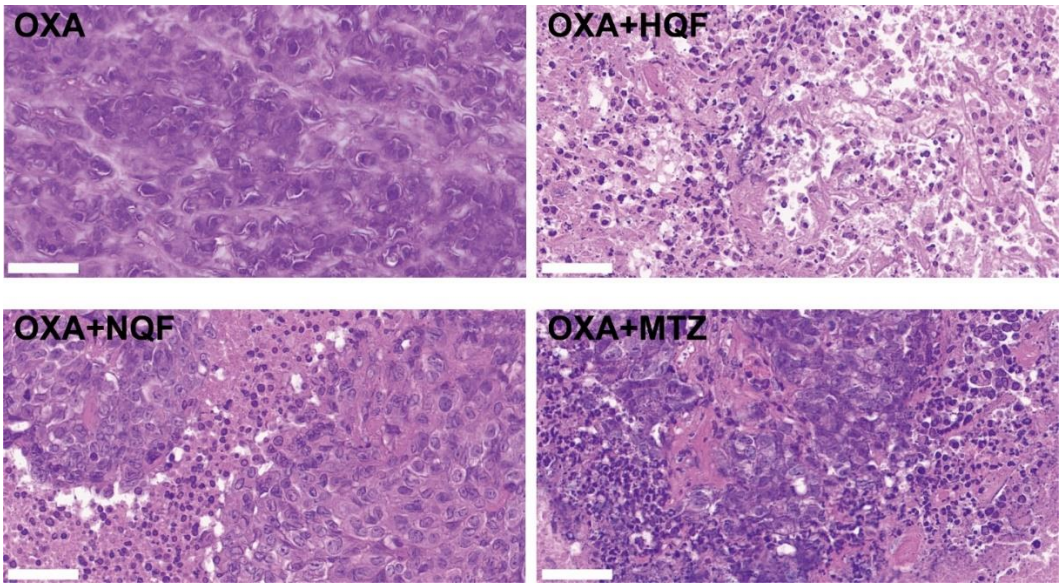

Fig. S23. H&E staining of tumor tissues with different treatments. (Scale bars: 50 μm)

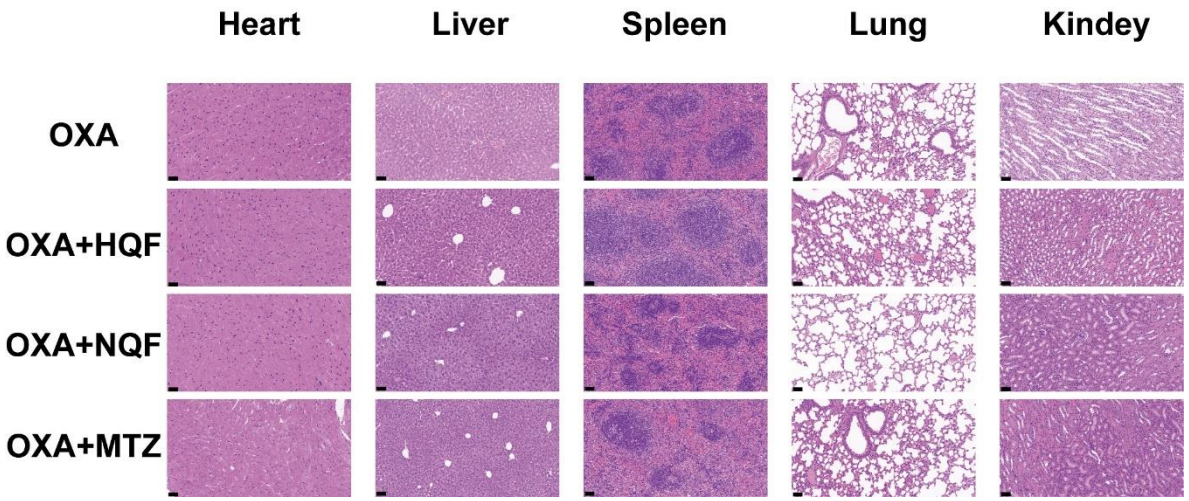

Fig. S24. H&E staining of typical major organs with different treatments. (Scale bars: 50 μm)

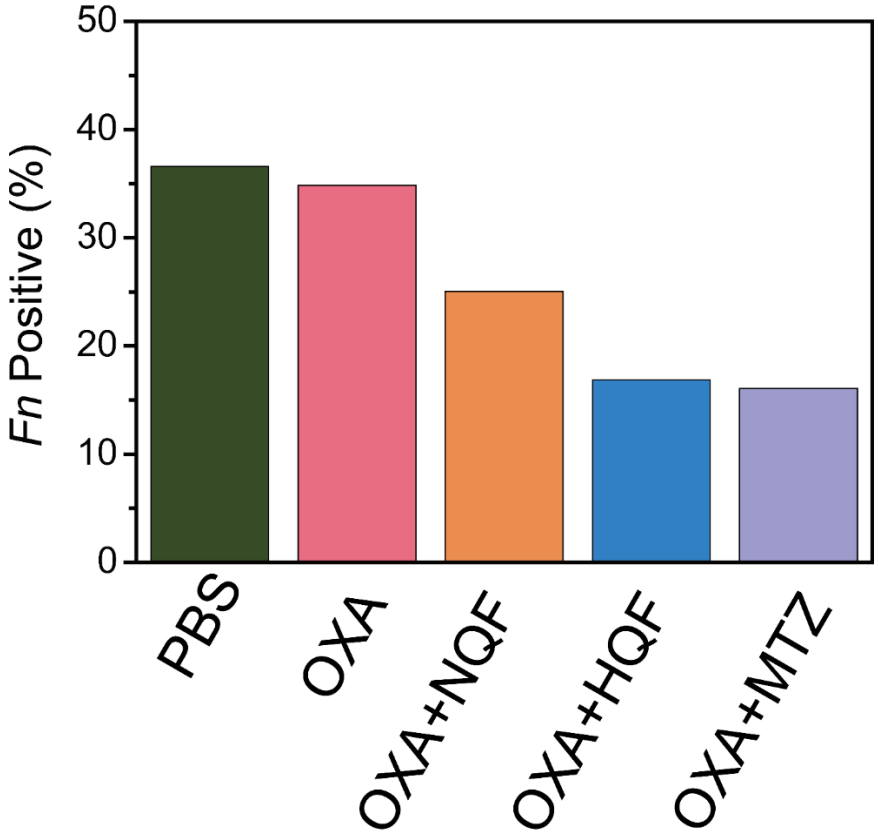

Fig S25. *F. nucleatum* positive values for panels in Fig 7G.

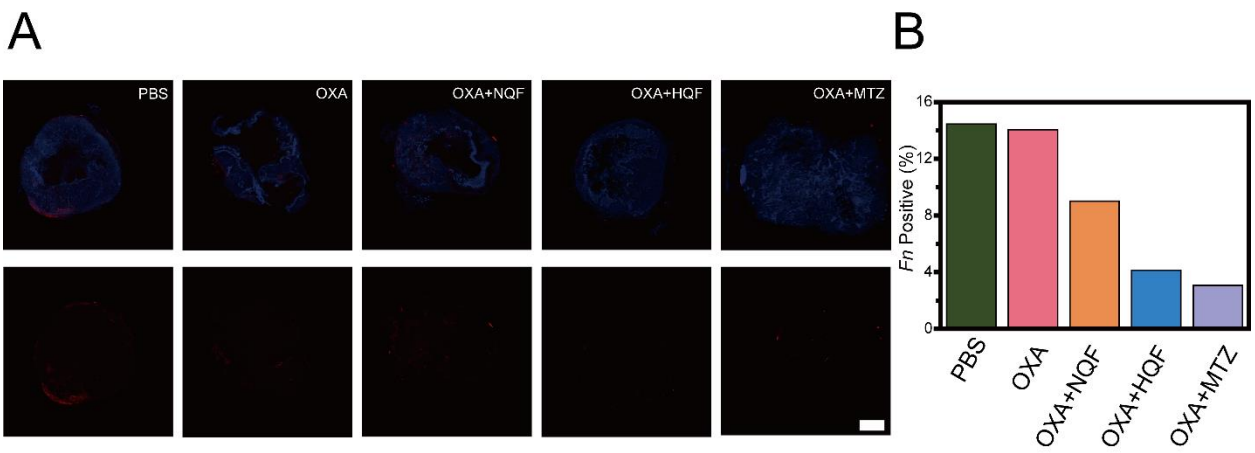

Fig. S26. (**A**) FISH staining of *F. nucleatum* (red) in tumor tissues sections (blue). (**B**) *F. nucleatum* positive values for panels in (**A**). (Scale bar: 2 mm)

3. ^{1}H-NMR spectra

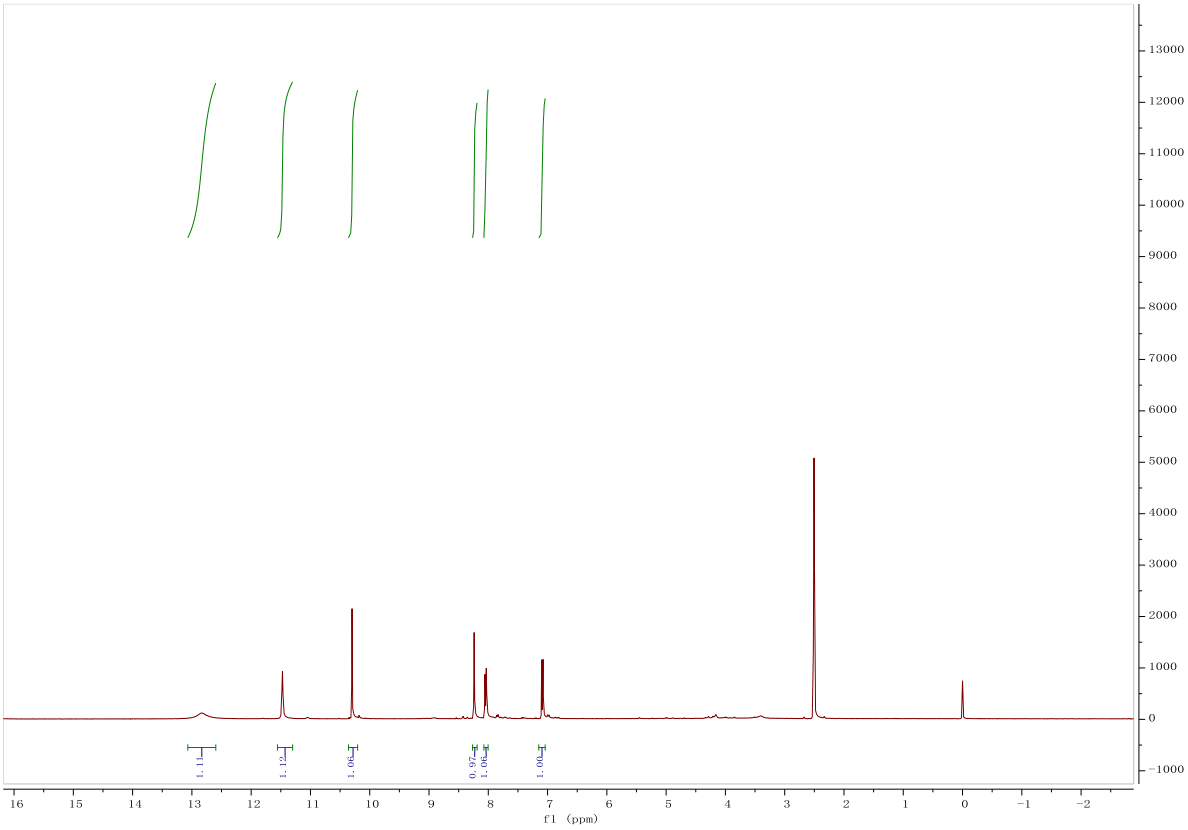

Fig. S27. ^{1}H-NMR of compound **1**.

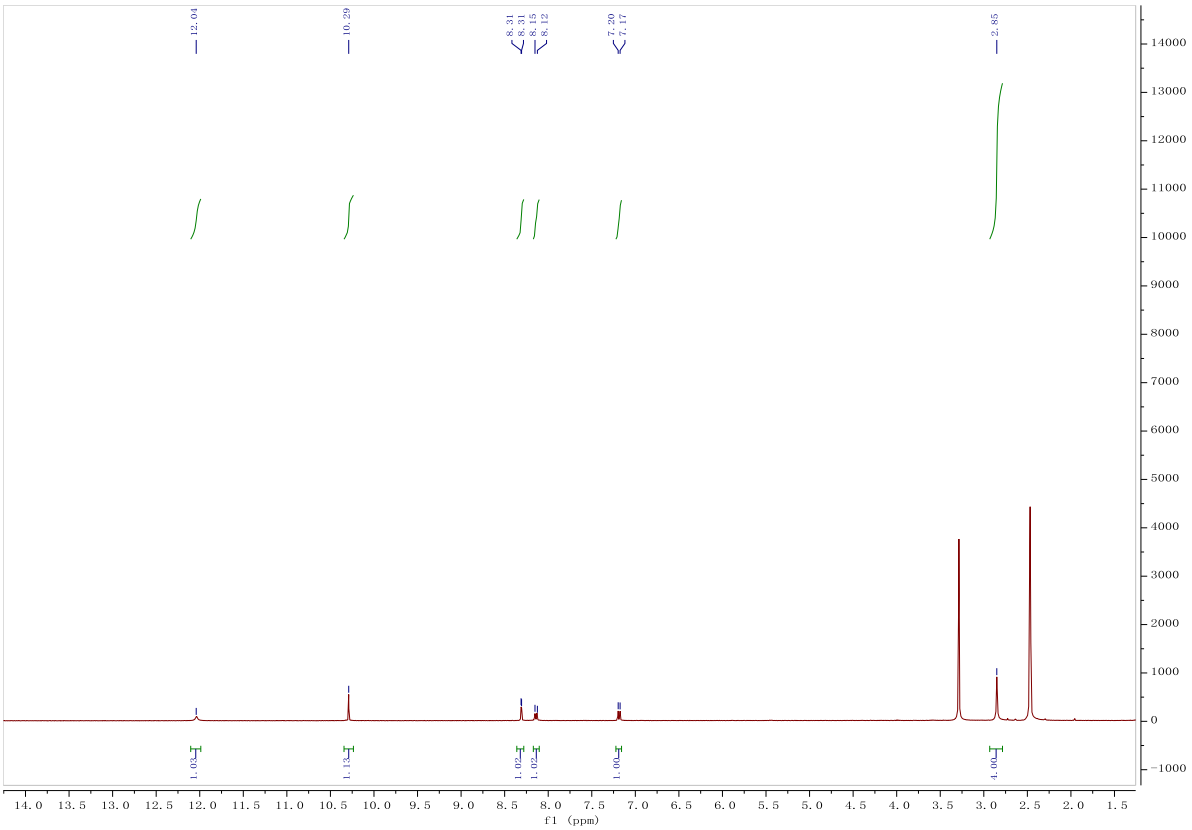

Fig. S28. ^{1}H-NMR of compound **2**.

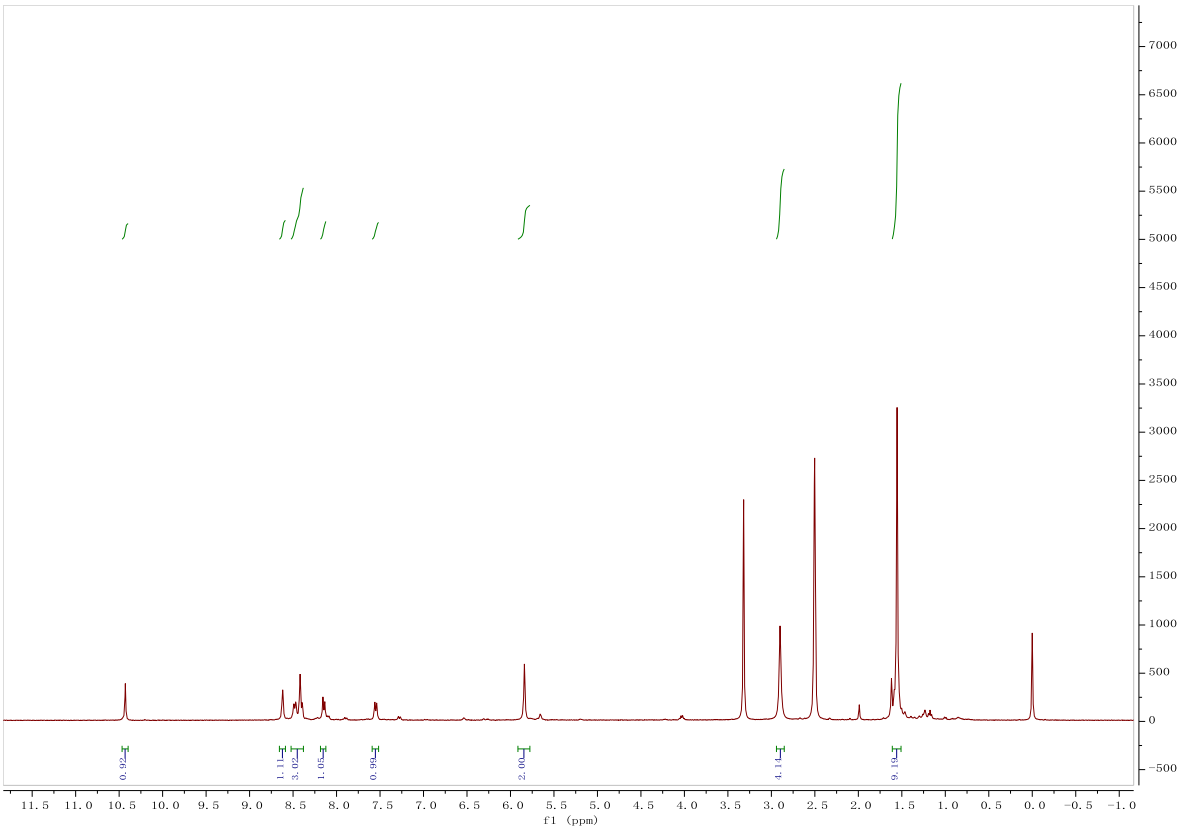

Fig. S29. ^{1}H-NMR of compound **3**.

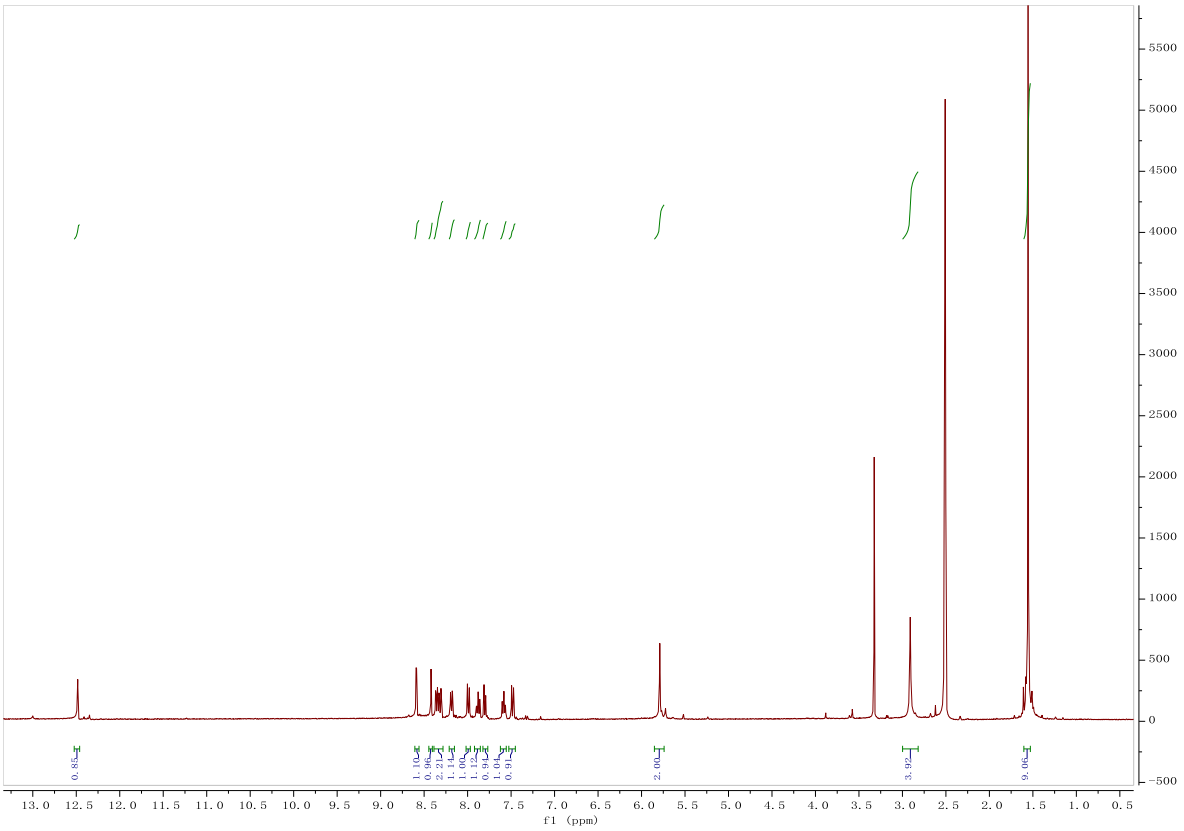

Fig. S30. ^{1}H-NMR of compound **4**.

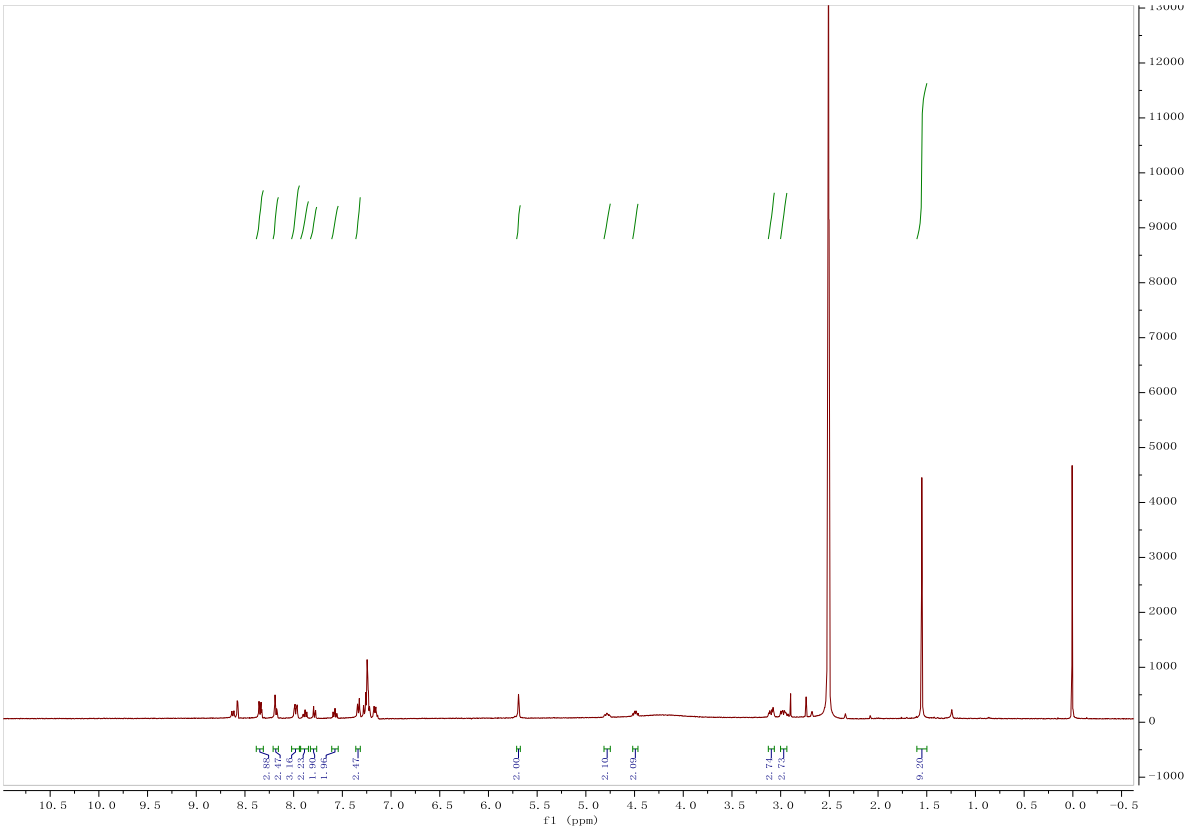

Fig. S31. ^{1}H-NMR of compound **5a**.

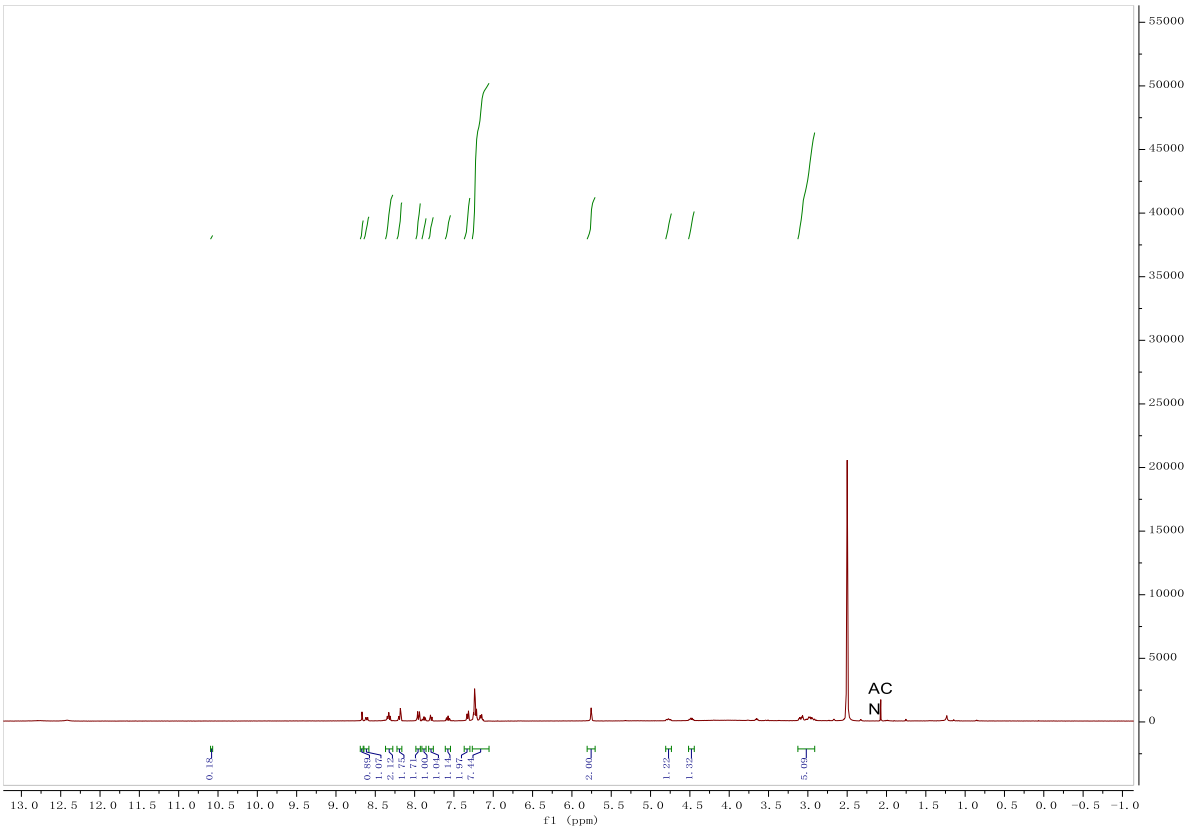

Fig. S32. ^{1}H-NMR of **NQF**.

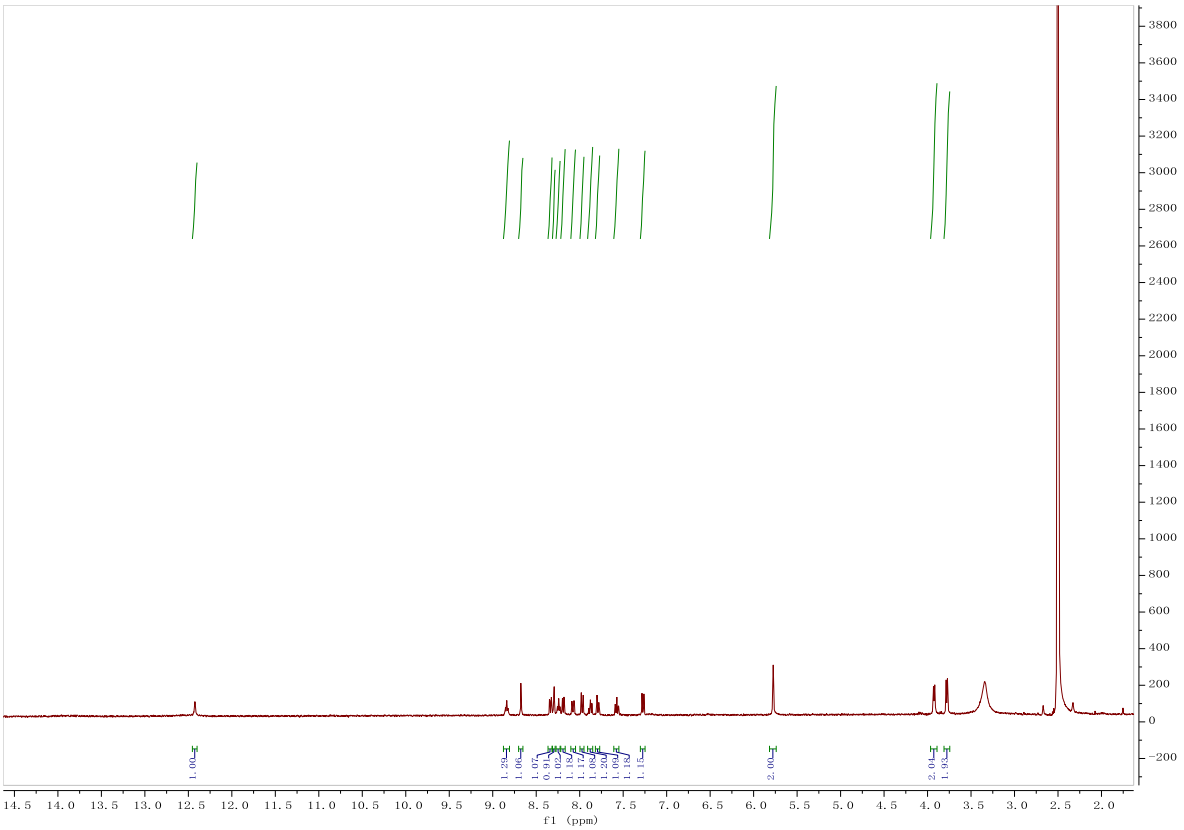

Fig. S33. ^{1}H-NMR of compound **NQG**.

4. Supplementary Table

Table S1. HPLC condition for the analysis of reduction reactions in Fig 3B. Fig 4E, Fig S4D and Fig S5.

Time (min)	Flow (mL/min)	H_2O (V %)	CH_3CN (V %)
0.01	1.0	60	40
20	1.0	30	70
30	1.0	0	100
35	1.0	60	40

REFERENCES AND NOTES

1. H. Sung, J. Ferlay, R. L. Siegel, M. Laversanne, I. Soerjomataram, A. Jemal, F. Bray, Global cancer statistics 2020: Globocan estimates of incidence and mortality worldwide for 36 cancers in 185 countries. *CA Cancer J. Clin.* **71**, 209–249 (2021).

2. E. Dekker, P. J. Tanis, J. L. A. Vleugels, P. M. Kasi, M. B. Wallace, Colorectal cancer. *Lancet* **394**, 1467–1480 (2019).

3. I. Dagogo-Jack, A. T. Shaw, Tumour heterogeneity and resistance to cancer therapies. *Nat. Rev. Clin. Oncol.* **15**, 81–94 (2018).

4. A. Janney, F. Powrie, E. H. Mann, Host-microbiota maladaptation in colorectal cancer. *Nature* **585**, 509–517 (2020).

5. M. Castellarin, R. L. Warren, J. D. Freeman, L. Dreolini, M. Krzywinski, J. Strauss, R. Barnes, P. Watson, E. Allen-Vercoe, R. A. Moore, R. A. Holt, *Fusobacterium nucleatum* infection is prevalent in human colorectal carcinoma. *Genome Res.* **22**, 299–306 (2012).

6. A. D. Kostic, E. Chun, L. Robertson, J. N. Glickman, C. A. Gallini, M. Michaud, T. E. Clancy, D. C. Chung, P. Lochhead, G. L. Hold, E. M. El-Omar, D. Brenner, C. S. Fuchs, M. Meyerson, W. S. Garrett, *Fusobacterium nucleatum* potentiates intestinal tumorigenesis and modulates the tumor-immune microenvironment. *Cell Host Microbe* **14**, 207–215 (2013).

7. K. Mima, R. Nishihara, Z. R. Qian, Y. Cao, Y. Sukawa, J. A. Nowak, J. H. Yang, R. X. Dou, Y. Masugi, M. Song, A. D. Kostic, M. Giannakis, S. Bullman, D. A. Milner, H. Baba, E. L. Giovannucci, L. A. Garraway, G. J. Freeman, G. Dranoff, W. S. Garrett, C. Huttenhower, M. Meyerson, J. A. Meyerhardt, A. T. Chan, C. S. Fuchs, S. Ogino, *Fusobacterium nucleatum* in colorectal carcinoma tissue and patient prognosis. *Gut* **65**, 1973–1980 (2016).

8. S. Bullman, C. S. Pedamallu, E. Sicinska, T. E. Claney, X. Y. Zhang, D. N. Cai, D. Neuberg, K. Huang, F. Guevara, T. Nelson, O. Chipashvili, T. Hagan, M. Walker, A. Ramachandran, B. Diosdado, G. Serna, N. Mulet, S. Landolfi, S. Ramon y Cajal, R. Fasani, A. J. Aguirre, K. Ng, E. Elez, S.

Ogino, J. Tabernero, C. S. Fuchs, W. C. Hahn, P. Nuciforo, M. Meyerson, Analysis of *Fusobacterium* persistence and antibiotic response in colorectal cancer. *Science* **358**, 1443–1448 (2017).

9. T. Yu, F. Guo, Y. Yu, T. Sun, D. Ma, J. Han, Y. Qian, I. Kryczek, D. Sun, N. Nagarsheth, Y. Chen, H. Chen, J. Hong, W. Zou, J.-Y. Fang, *Fusobacterium nucleatum* promotes chemoresistance to colorectal cancer by modulating autophagy. *Cell* **170**, 548–563.e16 (2017).

10. W. T. Song, K. Tiruthani, Y. Wang, L. M. Shen, M. Y. Hu, O. Dorosheva, K. Y. Qiu, K. A. Kinghorn, R. H. Liu, L. Huang, Trapping of lipopolysaccharide to promote immunotherapy against colorectal cancer and attenuate liver metastasis. *Adv. Mater.* **30**, e1805007 (2018).

11. W. Song, A. C. Anselmo, L. Huang, Nanotechnology intervention of the microbiome for cancer therapy. *Nat. Nanotechnol.* **14**, 1093–1103 (2019).

12. J. C. Clemente, L. K. Ursell, L. W. Parfrey, R. Knight, The impact of the gut microbiota on human health: An integrative view. *Cell* **148**, 1258–1270 (2012).

13. D. W. Zheng, X. Dong, P. Pan, K. W. Chen, J. X. Fan, S. X. Cheng, X. Z. Zhang, Phage-guided modulation of the gut microbiota of mouse models of colorectal cancer augments their responses to chemotherapy. *Nat. Biomed. Eng.* **3**, 717–728 (2019).

14. D. A. Salick, J. K. Kretsinger, D. J. Pochan, J. P. Schneider, Inherent antibacterial activity of a peptide-based beta-hairpin hydrogel. *J. Am. Chem. Soc.* **129**, 14793–14799 (2007).

15. B. Hu, C. Owh, P. Chee, W. Leow, X. Liu, Y.-L. Wu, P. Guo, X. J. Loh, X. Chen, Supramolecular hydrogels for antimicrobial therapy. *Chem. Soc. Rev.* **47**, 6917–6929 (2018).

16. L. Schnaider, S. Brahmachari, N. W. Schmidt, B. Mensa, S. Shaham-Niv, D. Bychenko, L. Adler-Abramovich, L. J. W. Shimon, S. Kolusheva, W. F. DeGrado, E. Gazit, Self-assembling dipeptide antibacterial nanostructures with membrane disrupting activity. *Nat. Commun.* **8**, 1365 (2017).

17. Z. Huang, Y. Liu, L. Wang, A. Ali, Q. Yao, X. Jiang, Y. Gao, Supramolecular assemblies mimicking neutrophil extracellular traps for mrse infection control. *Biomaterials* **253**, 120124 (2020).

18. T. Kinouchi, Y. Manabe, K. Wakisaka, Y. Ohnishi, Biotransformation of 1-nitropyrene in intestinal anaerobic bacteria. *Microbiol. Immunol.* **26**, 993–1005 (1982).

19. Q. X. Yao, Z. T. Huang, D. D. Liu, J. L. Chen, Y. Gao, Enzyme-instructed supramolecular self-assembly with anticancer activity. *Adv. Mater.* **31**, 1804814 (2019).

20. S. Chagri, D. Y. W. Ng, T. Weil, Designing bioresponsive nanomaterials for intracellular self-assembly. *Nat. Rev. Chem.* **6**, 320–338 (2022).

21. Z. Huang, Q. Yao, J. Chen, Y. Gao, Redox supramolecular self-assemblies nonlinearly enhance fluorescence to identify cancer cells. *Chem. Commun.* **54**, 5385–5388 (2018).

22. Y. Kuang, M. J. C. Long, J. Zhou, J. F. Shi, Y. Gao, C. Xu, L. Hedstrom, B. Xu, Prion-like nanofibrils of small molecules (PriSM) selectively inhibit cancer cells by impeding cytoskeleton dynamics. *J. Biol. Chem.* **289**, 29208–29218 (2014).

23. S. N. Moreno, R. P. Mason, R. Docampo, Reduction of nifurtimox and nitrofurantoin to free radical metabolites by rat liver mitochondria. Evidence of an outer membrane-located nitroreductase. *J. Biol. Chem.* **259**, 6298–6305 (1984).

24. A. Chevalier, Y. Zhang, O. M. Khdour, J. B. Kaye, S. M. Hecht, Mitochondrial nitroreductase activity enables selective imaging and therapeutic targeting. *J. Am. Chem. Soc.* **138**, 12009–12012 (2016).

25. M. M. Zhang, Y. Guan, Z. Dang, P. G. Zhang, Z. Zheng, L. Chen, W. Kuang, C. C. Wang, G. L. Liang, Directly observing intracellular nanoparticle formation with nanocomputed tomography. *Sci. Adv.* **6**, eaba3190 (2020).

26. V. R. Sinha, R. Kumria, Colonic drug delivery: Prodrug approach. *Pharm. Res.* **18**, 557–564 (2001).

27. X. B. Zhao, W. Ha, K. Gao, Y. P. Shi, Precisely traceable drug delivery of azoreductase-responsive prodrug for colon targeting via multimodal imaging. *Anal. Chem.* **92**, 9039–9047 (2020).

28. M. Li, Y. Zhang, X. Ren, W. Niu, Q. Yuan, K. Cao, J. Zhang, X. Gao, D. Su, Activatable fluorogenic probe for accurate imaging of ulcerative colitis hypoxia in vivo. *Chem. Commun.* **58**, 819–822 (2022).

29. J. Abed, J. E. M. Emgard, G. Zamir, M. Faroja, G. Almogy, A. Grenov, A. Sol, R. Naor, E. Pikarsky, K. A. Atlan, A. Mellul, S. Chaushu, A. L. Manson, A. M. Earl, N. Ou, C. A. Brennan, W. S. Garrett, G. Bachrach, Fap2 mediates fusobacterium nucleatum colorectal adenocarcinoma enrichment by binding to tumor-expressed gal-galnac. *Cell Host Microbe* **20**, 215–225 (2016).

30. P. E. Kolenbrander, R. N. Andersen, Inhibition of coaggregation between fusobacterium nucleatum and porphyromonas (bacteroides) gingivalis by lactose and related sugars. *Infect. Immun.* **57**, 3204–3209 (1989).

31. S. Coppenhagen-Glazer, A. Sol, J. Abed, R. Naor, X. Zhang, Y. W. Han, G. Bachrach, Fap2 of fusobacterium nucleatum is a galactose-inhibitable adhesin involved in coaggregation, cell adhesion, and preterm birth. *Infect. Immun.* **83**, 1104–1113 (2015).

32. N. K. Saini, A. Baena, T. W. Ng, M. M. Venkataswamy, S. C. Kennedy, S. Kunnath-Velayudhan, L. J. Carreno, J. Xu, J. Chan, M. H. Larsen, W. R. Jacobs, Jr., S. A. Porcelli, Suppression of autophagy and antigen presentation by mycobacterium tuberculosis pe_pgrs47. *Nat. Microbiol.* **1**, 16133 (2016).

33. H. He, W. Tan, J. Guo, M. Yi, A. Shy, B. Xu, Enzymatic noncovalent synthesis. *Chem. Rev.* **120**, 9994–10078 (2020).

34. Z. M. Yang, K. M. Xu, Z. F. Guo, Z. H. Guo, B. Xu, Intracellular enzymatic formation of nanofibers results in hydrogelation and regulated cell death. *Adv. Mater.* **19**, 3152–3156 (2007).

35. Y. Gao, J. Shi, D. Yuan, B. Xu, Imaging enzyme-triggered self-assembly of small molecules inside live cells. *Nat. Commun.* **3**, 1033 (2012).

36. V. Béreau, V. Jubéra, P. Arnaud, A. Kaiba, P. Guionneau, J.-P. Sutter, Modulation of the luminescence quantum efficiency for blue luminophor $\{Al(salophen)\}^+$ by ester-substituents. *Dalton Trans.* **39**, 2070–2077 (2010).

37. K. Moeity, K. Tanizawa, Y. Kanaoka, Schiff base copper(II) chelate as a tool for immobilization of protein. *Chem. Pharm. Bull.* **37**, 2849–2851 (1989).